Nanoscale

REVIEW

View Article Online
View Journal | View Issue

Cite this: *Nanoscale*, 2024, **16**, 18684

Advanced approaches in skin wound healing – a review on the multifunctional properties of MXenes in therapy and sensing

Valeria Ferrara,†[a] Caterina Perfili,†[a] Giulia Artemi,[b] Brunella Iacolino,[b] Francesca Sciandra,[c] Giordano Perini,[a,d] Laura Fusco,[e] Maksym Pogorielov,[f,g] Lucia Gemma Delogu,[h,e] Massimiliano Papi, *[a,b,d] Marco De Spirito*[a,d] and Valentina Palmieri [a,b,d]

Received 9th July 2024,
Accepted 11th September 2024

DOI: 10.1039/d4nr02843k

rsc.li/nanoscale

In recent years, the use of MXenes, a class of two-dimensional materials composed of transition metal carbides, nitrides, or carbonitrides, has shown significant promise in the field of skin wound healing. This review explores the multifunctional properties of MXenes, focusing on their electrical conductivity, photothermal effects, and biocompatibility in this field. MXenes have been utilized to develop advanced wound healing devices such as hydrogels, patches, and smart bandages for healing examination. These devices offer enhanced antibacterial activity, promote tissue regeneration, and provide real-time monitoring of parameters. The review highlights the synthesis methods, chemical features, and biological effects of MXenes, emphasizing their role in innovative skin repair strategies. Additionally, it discusses the potential of MXene-based sensors for humidity, pH, and temperature monitoring, which are crucial for preventing infections and complications in wound healing. The integration of MXenes into wearable devices represents a significant advancement in wound management, promising improved clinical outcomes and enhanced quality of life for patients.

1. Introduction

Skin wound healing is a delicate and coordinated multistep process that might fail because of systemic or local factors that disrupt the microenvironment, hinder the repair progression, and potentially lead to chronic or non-healing wounds. With the rising cost of treatments each year, skin wounds affect millions of people worldwide. As a sort of "silent epidemic", the mortality rate of chronic diabetic foot ulcers is around 30%, similar to cancer.[1] Therefore, efficient wound healing to restore the injured site to its normal state is crucial and urgent.

In general, skin wound therapies are classified into "conventional" or "regenerative". Conventional wound therapies involve infection control through regular dressing changes and weekly debridement of damaged tissues. For large or full-thickness skin defects, split-thickness skin autografts are commonly used. Autografts come with drawbacks such as the need for multiple surgical interventions, limited availability, hypertrophic scarring, and possible functional alterations. In contrast, regenerative wound healing leverages advanced biomedical research technologies such as stem cell and gene therapy, targeted drug/growth factor delivery, and bioengineered skin grafts. These approaches aim to restore the original function of the skin and repair damaged tissues effectively, resulting in improved wound healing without scarring. Early strategies focused on regenerating the skin's layer-by-layer structure using bioengineered scaffolds or hydrogels encapsulated with cells.[1] As our understanding of the healing process has grown, the focus of chronic wound treatment has shifted from simple debridement and topical dressing to more

[a]*Fondazione Policlinico Universitario "A. Gemelli" IRCSS, L.go Agostino Gemelli 8, 00136 RM, Rome, Italy. E-mail: Massimiliano.papi@unicatt.it, marco.despirito@unicatt.it*
[b]*Istituto dei Sistemi Complessi, ISC-CNR, Via dei Taurini 19, 00185, RM, Rome, Italy*
[c]*Istituto di Scienze e Tecnologie Chimiche "Giulio Natta", SCITEC-CNR, c/o Istituto Biochimica e Biochimica Clinica, Università Cattolica del Sacro Cuore, L.go Vito, 1, 00168 RM, Rome, Italy*
[d]*Dipartimento di Neuroscienze, Università Cattolica del Sacro Cuore, L. go Francesco Vito, 1, 00168 RM, Rome, Italy*
[e]*ImmuneNanoLab, Dipartimento di Scienze Biomediche, Università degli Studi di Padova, Padova, Italy*
[f]*Biomedical Research Centre, Sumy State University, Kharkivska Street, 116, 40007 Sumy, Ukraine*
[g]*Institute of Atomic Physics and Spectroscopy, University of Latvia, Jelgavas street, 3, Riga, 1004, Latvia*
[h]*RIC2D, Department of Biological Sciences, Khalifa University of Science & Technology, Abu Dhabi, United Arab Emirates*
†These authors equally contributed.

advanced microenvironment therapy, using biomaterials and nanomaterials to achieve unprecedented effects.

MXenes are a class of two-dimensional materials composed of transition metal carbides, nitrides, or carbonitrides, known for their excellent electrical conductivity, mechanical strength, and versatility in various applications such as energy storage, sensors, and biomedical devices. In this Review, we will focus on the use of MXenes nanomaterials in the field of skin regeneration, and how the electrical and photothermal properties of MXenes have induced the design of multifunctional devices for therapy and sensing.

In section 1, we describe the synthesis methods and chemical features of MXenes with a specific highlight on light absorptivity and electrical conductivity. In section 2, we describe generically the biological effects of MXenes on eukaryotic and prokaryotic cells. After describing the general mechanism of skin repair (section 3), we move to patches and hydrogels specifically designed for wound healing, indeed even if many studies on antibacterial and regenerative properties of MXenes are available,[2,3] we will focus on those devices that have been designed for skin diseases, including melanoma, chronic and diabetic wounds. MXenes, with their high conductivity and versatility, have garnered significant interest in the field of sensors,[4] in section 5 of this Review, we focus on MXene-based sensors that combine wound healing properties with wound monitoring capabilities. Humidity sensors can provide real-time moisture monitoring of wounds – which is crucial for preventing infections and complications, pH sensors indicate healing progress and infection, and temperature sensors signal inflammation. These technologies, based on the unique properties of MXenes, create multifunctional platforms that facilitate wound healing and provide real-time monitoring of critical wound parameters. Integrating these functions into wearable devices and smart bandages represents a significant advancement in wound management, promising improved clinical outcomes and enhanced quality of life for patients.

2. MXenes chemical structure and properties

MXenes are two-dimensional (2D) materials defined by the general formula $M_{n+1}X_nT_x$, where M is a transition metal, X corresponds to carbon or nitrogen, T denotes a surface-terminating functional group (OH, F, O, H, *etc.*) and n is an integer with a value ranging from 1 to 3.[5] The M–X bonds consist of a mixture of covalent, metallic, and ionic bonds which make them appealing for many applications.[6]

The first synthesis of MXenes dates to 2011, when Prof. Yuri Gogotsi and coworkers carried out the exfoliation of $Ti_3C_2T_x$, which led to the production of 2D nanocrystals $Ti_3C_2T_x$.[7]

The bidimensional MXenes are obtained from a precursor three-dimensional (3D) MAX phase,[8] hexagonal layered transition metal carbides and nitrides with a generic formula of $M_{n+1}AX_n$ (n = 1, 2 or 3), where M is an early transition metal, A is an element from groups 13 and 14 in the periodic table and X is carbon or nitrogen.[9] The periodic table in Fig. 1A from ref. 10 illustrates the elements used in MAX phases and MXenes.

Different synthetic strategies have been explored in recent years and can be divided mainly into two approaches: *top-down* and *bottom-up* approaches. The top-down pathway consists of selective etching from MAX or non-MAX Phases. General etchants used for production contain fluoride ions, such as hydrofluoric acid (HF). Naguib *et al.* reported the exfoliation of $Ti_3C_2T_x$ powder using an HF solution, followed by washing with deionized water and centrifugation to obtain the desired product Ti_3C_2.[7]

The use of fluoride-containing etchants is due to the strong metallic bonds between the 'M' and 'A' elements, which could not be separated by mechanical exfoliation. In addition, MXenes derived by selective HF etching may carry different terminations on their surfaces (*i.e.*, OH, H, O, F, *etc.*) which are generally referred to as T_x in the general formula $M_{n+1}X_nT_x$. The HF concentration and etching time increases as the increment of M atomic number, which can be attributed to the stronger M–Al bonding: a larger number of M valence electrons requires stronger etching to break the metallic M–A bonds.[6] Different milder and safer bifluoride etchants have been explored (such as NH_4HF_2, $NaHF_2$, and KHF_2).[12] Interestingly, it has been discovered that MXenes can also be obtained from non-MAX phases, such as Mo_2Ga_2C.[13] As a result of exfoliation treatment, solid dense MAX particles are converted to a loosely packed accordion-like layered structure.[6]

The bottom-up strategies involve different techniques, among which the most common method is represented by chemical vapour deposition.[14] Fig. 1B from ref. 11 effectively shows the transformation from MAX precursors to MXenes. When the number of stacked layers is less than 5, the few-layer MXenes (FL-MX) nomenclature is generally used. Otherwise, they can be referred to as multi-layer MXenes (ML-MX), with selective biological properties depending on the layer number.[15] Given the wide range of different combinations possible, different MXenes, such as Ti_3C_2, Ti_2C, Nb_2C, V_2C, Ti_3CN, Mo_2C, and Ta_4C_3 (see Fig. 2 from ref. 11) have been synthesized to date, among which $Ti_3C_2T_x$ is the most common and well-studied MXenes in the medical field.

Electrical conductivity is thought to be one of the most exploitable properties of MXenes for the near future, especially for its use in optoelectronic-based devices, health sensors, and wearable thermoelectric devices.

Electrical conductivity is directly linked to the chemical morphology of MXenes[16,17] according to specific features: (i) mono-layer, few-layers, or multi-layers structure, (ii) different light or heavy transition metals of the M element, (iii) the thickness of MXenes monolayer, (iv) the synthesis conditions and/or the post-etching treatment and (v) the functional groups attached to the surface.[16,17]

The ability of some materials, including MXenes, to convert light into heat – generally known as the photothermal effect – is particularly appealing in the biomedical sector. This property can be exploited to carry out specific anti-cancer and anti-

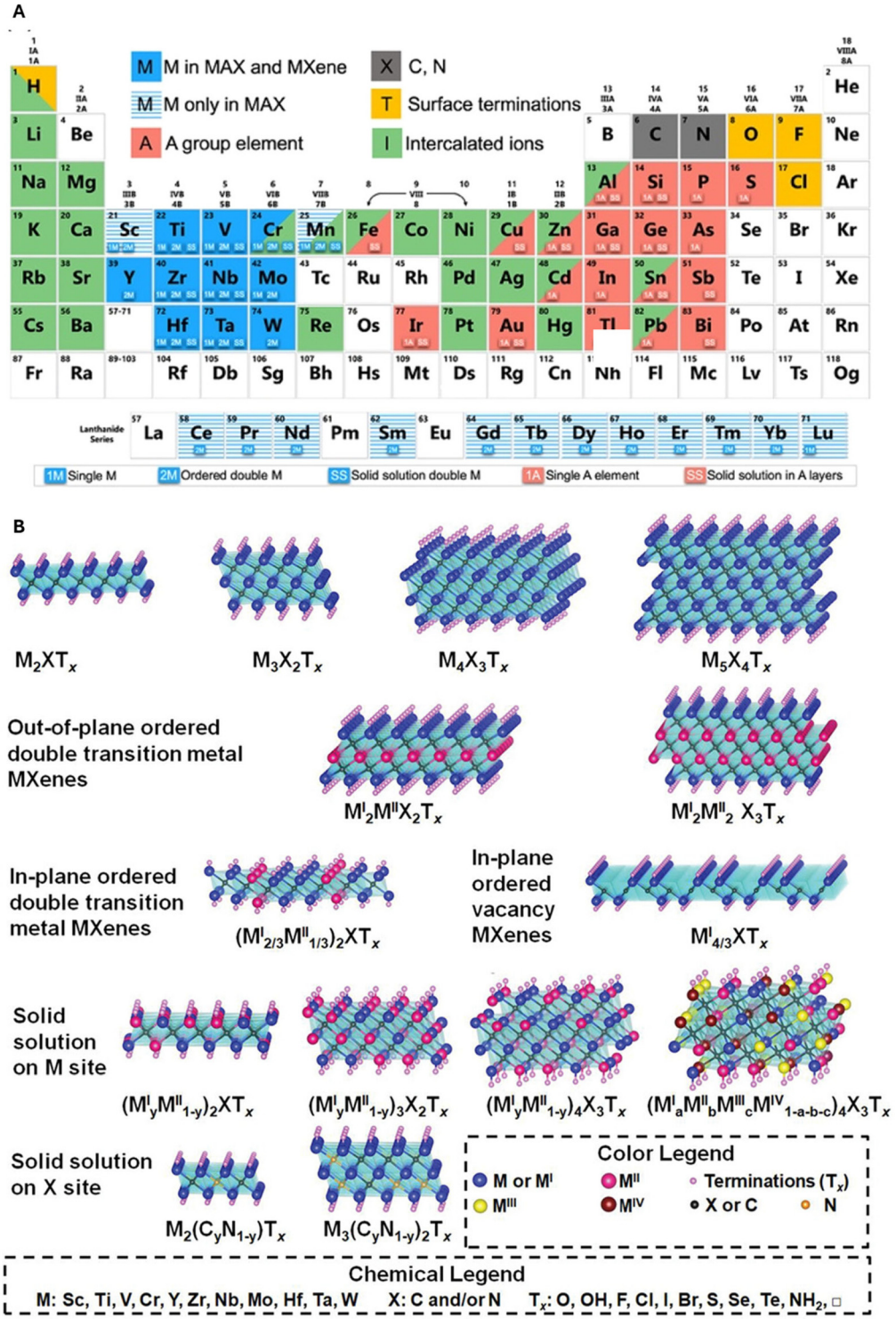

Fig. 1 (A) Periodic table of elements used for MAX phases and MXenes. The periodic table highlighting elements used in MAX phases and MXenes. Elements in striped light blue are utilized in MAX phases, while those in blue are found in both MXenes and MAX phases. Dark grey elements represent carbon and nitrogen. Intercalated ions and surface functional groups are depicted in green and yellow, respectively. Adapted with permission from ref. 10. Copyright 2019 American Chemical Society. (B) Scheme shows the transformation from MAX precursors to MXenes. The A element is eliminated through the selective etching process, which leads to the introduction of T_x functional groups. The bone structure formed by carbide (or nitride) elements and transition metals remains constant. Reproduced with permission from ref. 11. Copyright 2021 Wiley-VCH GmbH.

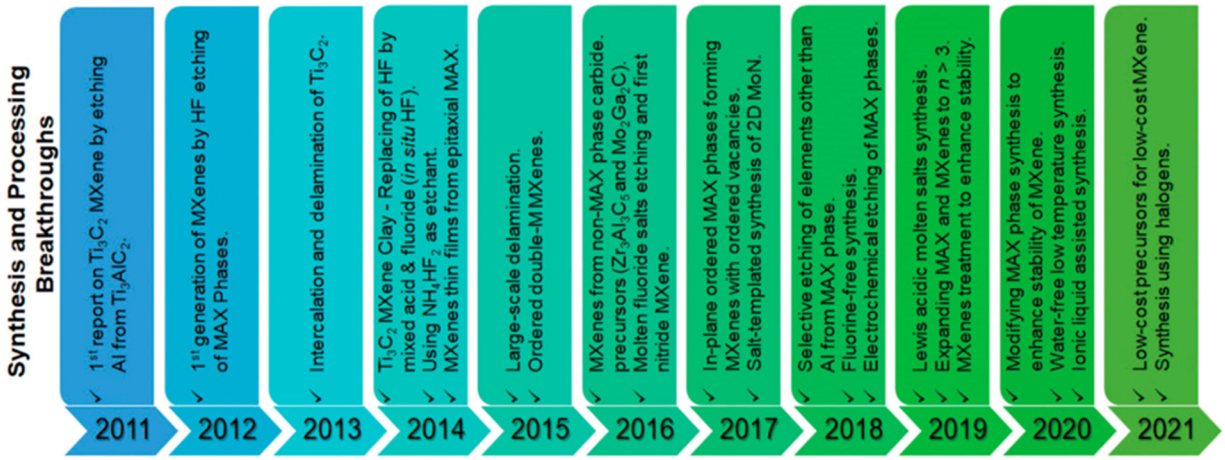

Fig. 2 Illustration of chronological production of MXenes from 2011 to 2021. Modified with permission from ref. 11. Copyright 2021 Wiley-VCH GmbH.

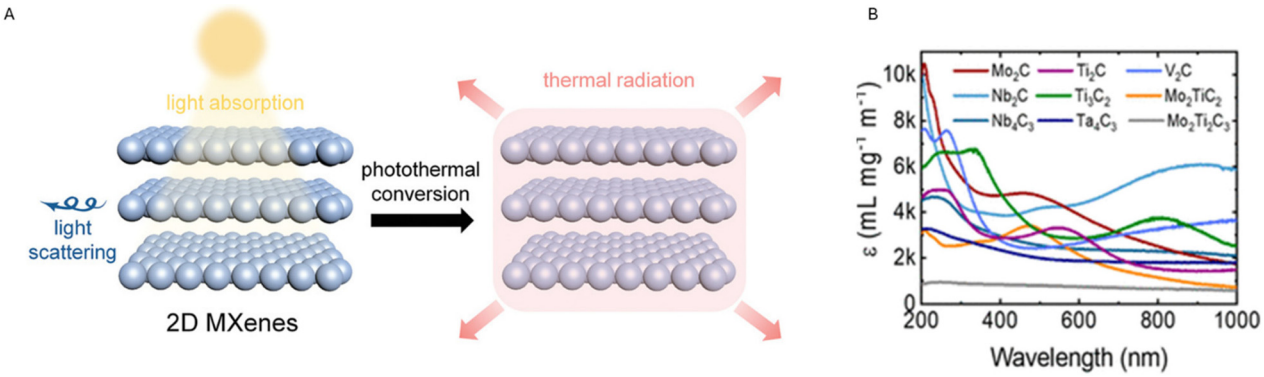

Fig. 3 (A) Illustration of the photothermal conversion exhibited by 2D MXenes. Reproduced with permission from ref. 19. Copyright 2020 Wiley Online Library. (B) Illustrates the extinction coefficient ε (L g^{-1} cm^{-1}) *vs.* wavelength (nm) for different MXenes. The extinction coefficient – also referred to as the 'mass attenuation coefficient' – represents how deeply a material can be penetrated by a beam of electromagnetic radiation. This coefficient can be indicated by L g^{-1} cm^{-1}, and related multiples or submultiples, to describe materials in solution. (NIR wavelength is in the range of 780 to 2500 nm). Reproduced with permission from ref. 20. Copyright 2022 American Chemical Society.

bacterial treatments, such as Photodynamic Therapy (PDT) and Photothermal Therapy (PTT)[18] (Fig. 3).

During photothermal conversion, a photon coming from a specific electromagnetic radiation hits the material's surface and is absorbed by the material itself. This leads to photo-excitation (*i.e.*, movements of electrons), eventually resulting in heat production. Different mechanisms have been suggested to explain the photothermal conversion and the most occurrent has been reported to be: (a) localized surface plasmon resonance (LSPR) effect, (b) electron–hole effect and (c) conjugation or hyperconjugation effect.[19] The LSPR effect occurs when the electrons on the material's surface exhibit the same frequency as the photon hitting the surface. When the oscillation is resonant, the subsequent decay might follow two alternative pathways: one radiative process re-emits photons and can lead to light scattering, while during the other non-radiative process hot electrons – resulting from excitation – are hypothesized to be translated into thermal energy that rises the surrounding temperature by the vibration of lattice scattering.[19] The LSPR effect is usually observed in metal nanoparticles[21] however, according to recent studies, this effect might also explain the photothermal mechanism in the specific case of MXenes.[22] Also, the LSPR effect seems to happen, especially in the near-infrared (NIR) region, which is the region used for PDT and PTT, thus confirming the promising potentialities of MXenes in the biomedical field. NIR can deeply penetrate biological tissues due to the low absorption of NIR light by hemoglobin and water.[15] Finally, MXenes have been shown to exhibit a high extinction coefficient (see Fig. 3B from ref. 20).

3. Toxicity of MXenes towards cells and bacteria

MXenes have recently attracted interest in the biomedical field, due to their low toxicity, high biocompatibility, and NIR

absorption capacity.[23] At present, MXene-based treatments are exploited to selectively destroy cancer cells and/or bacteria cells while limiting damage to healthy tissues.

To achieve a deeper insight into MXenes' toxicity, a distinction can be drawn between effects on eukaryotic cells or against bacteria. However, MXenes cell damage can be owed to three main mechanisms: (i) nano-knives effect; (ii) response to reactive oxygen species (ROS); (iii) additional factors (*i.e.*, surface modification, MXene synthesis method, exposure time, *etc.*), see Fig. 4 from ref. 24.

The "nano-knives effect" refers to the sharp shape that characterizes the edges of bidimensional MXenes' nanosheets. Their direct physical interaction results in damage both for the cellular plasma membrane and bacteria's wall, as previously described for other 2D materials such as graphene.[25] In the case of cells, the damage of cells' membrane can cause the outflow of cytoplasm in the outer environment.[24] This effect is enhanced in the case of few-layers MXenes compared to multilayer MXenes. FL-MXs have smaller dimensions, which makes it easier to enter the cell,[26,27] and the effect is amplified by the inability of cells to recover from damages caused by high concentrations of MXenes.[24]

The degree of toxicity depends on the cell line used for the tests, probably due to the different chemical composition and structure of the cell membrane, which is the main barrier against MXenes. Likewise in the case of bacteria, the "nano-knives effect" leads to the breakage of bacteria's outer envelopes.

Furthermore, a large interest has recently merged concerning the behavior of MXenes towards ROS species (Fig. 4). IT was shown that the chemical constituents of MXenes' structure influence the response of MXenes towards radical species, resulting in two different effects: ROS scavenging and ROS production. MXenes tend to produce radicals (such as superoxide anion $O_2^{\bullet -}$ and hydroxyl radical $HO^{\bullet}$) when they come in contact with O_2 and H_2O.[28] This pro-oxidant effect results to be increased when MXenes are irradiated with wavelengths belonging to the NIR spectrum,[29] which makes MXenes ideal candidates for PTT treatment of cancer. ROS species are positively exploited to specifically address cancer cells, leading to the damage and destruction of tumors.[30,31]

On the other hand, a specific type of MXenes based on niobium – Nb_2CT_x and $Nb_4C_3T_x$ – have recently shown the ability to spontaneously absorb and scavenge a considerable amount of ROS.[32] Regarding bacteria, ROS species exhibit a different effect depending on the chemical composition of bacteria walls of Gram-positive and Gram-negative bacteria. Gram-negative bacteria (*i.e.*, *E. coli*) have a peptidoglycan layer followed by an outer lipopolysaccharide membrane. This outer membrane is absent in Gram-positive bacteria (*i.e.*, *S. aureus*), that have the peptidoglycan layer as the most external.[33] Outer layers play a role in defending bacteria from ROS species produced in the outer environment. In the case of Gram-positive bacteria, the peptidoglycan layer efficiently inhibits the entrance of ROS species, while for Gram-negative bacteria, the lipopolysaccharide layer shows a higher susceptibility to ROS, since radicals might initiate radical chain reactions that lead to the production of endogenous ROS species. Although ROS species may impact with different intensity on Gram-positive and Gram-negative bacteria, a recent study showed that the

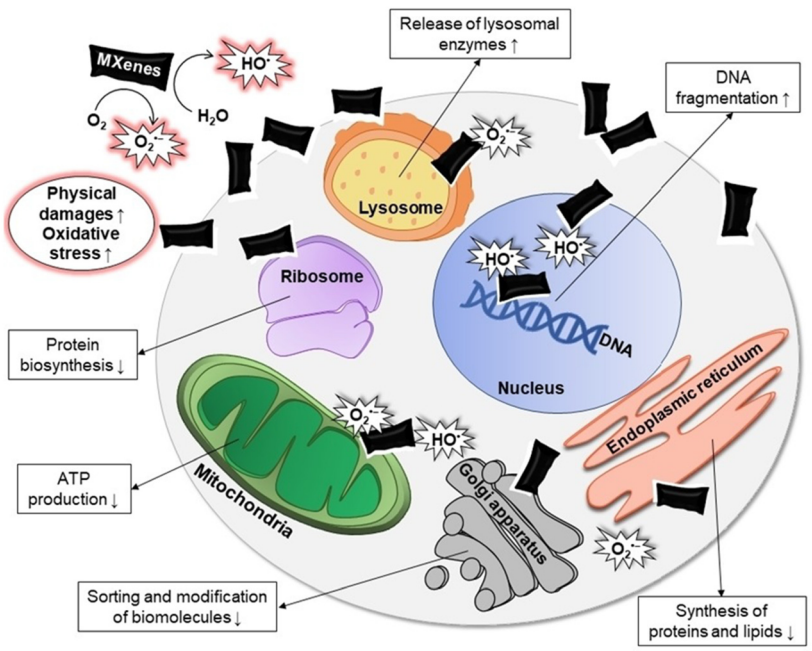

Fig. 4 Illustration of MXenes' toxicity to cells. The up-arrows describe an increasing effect (*i.e.* DNA fragmentation, release of lysosomal enzymes *etc.*), while the down-arrows show a decreased effect (*i.e.* protein biosynthesis, ATP production *etc.*). Reproduced with permission from ref. 24. Copyright 2024 Wiley-VCH GmbH.

effect of few-layer and ML-MX after NIR irradiation is comparable both against Gram-positive and Gram-negative bacteria.[15]

A list of further factors that affect MXenes toxicity comprises (i) surface modification: functional groups on MXenes' surface can result in an increased or decreased toxicity; (ii) the method of MXene synthesis might induce a toxic effect due to the presence of residues of etching agents, such as HF; (iii) the size: smaller MXenes have shown to be more cytotoxic since they can penetrate cells by endocytosis; (iv) dose and exposure time.[28]

4. Skin repair

4.1. General requirements for skin repair

Skin, whose general structure is depicted in Fig. 5A from ref. 1, represents the largest organ in the human body, the barrier between the body and the external environment.[34] The outermost layer of the skin (epidermis) consists of epithelial cells, although it also includes keratinocytes, melanocytes, Langerhans cells, and Merkel cells, among others.[35] Overall, the epidermis plays a crucial role in maintaining the body's homeostasis by regulating water loss and protecting against UV radiation and infection. Keratinocytes produce keratin which prevents water loss due to evaporation while by utilizing melanocytes the epidermis protects the skin from UV rays.[36] Tightly packed layers of keratinocytes, with the presence of specialized immune cells such as Langerhans cells, contribute to the skin's ability to defend against infections. The dermis is the intermediate layer of skin and is connected to the epidermis *via* the basement membrane composed of collagen, laminin, nidogenes, and proteoglycans, which form a complex reticular structure. The dermis provides structural support, hosts blood and lymphatic vessels, nerve endings, and various appendages, and is regulated by resident fibroblasts and macrophages.[37] Fibroblasts are responsible for the synthesis and the renewal of extracellular matrix made of carbohydrates and other molecules secreted by cells such as growth factors, cytokines, and enzymes, whereas macrophages contribute to eliminating foreign material and damaged tissue. The deepest skin layer, the hypodermis, is mainly composed of loose connective tissue and adipose tissue made of adipocytes. This inner layer provides nourishment through blood vessels that cope with nutrients and oxygen supply, including the dermis and epidermis; isolation through adipose tissue, which also helps to regulate body temperature; and energy reserve for the body since adipocytes store excess energy in the form of triglycerides.[35]

If a skin injury occurs, a four-stage repair process begins, encompassing the hemostatic, inflammatory, proliferative, and remodelling stages as shown in Fig. 5B from ref. 1. The exposure of vascular endothelial cells and the presence of exogenous molecules in the wound activate the coagulation cascade, leading to platelet activation, accumulation, and thrombus formation at the injury site.[38] The resulting platelet thrombus, along with fibrin and fibronectin, forms hemostatic insoluble clots that facilitate the attachment of immune cells. These immune cells release cytokines and inflammatory factors, which promote the migration and aggregation of additional inflammatory cells, thereby initiating the inflammatory response.[39] In addition to fostering inflammation and recruiting macrophages, neutrophils in the area engage in phagocytosis and release reactive oxygen species, antimicrobial peptides, and proteolytic enzymes to eliminate necrotic tissue and pathogens. As the inflammatory response progresses, macrophages transition from a pro-inflammatory to an anti-inflammatory phenotype, releasing various growth factors that encourage angiogenesis, fibroplasia, and keratinocyte re-epithelialization.[40]

During the proliferative stage, keratinocytes, fibroblasts, and endothelial cells proliferate under the influence of growth

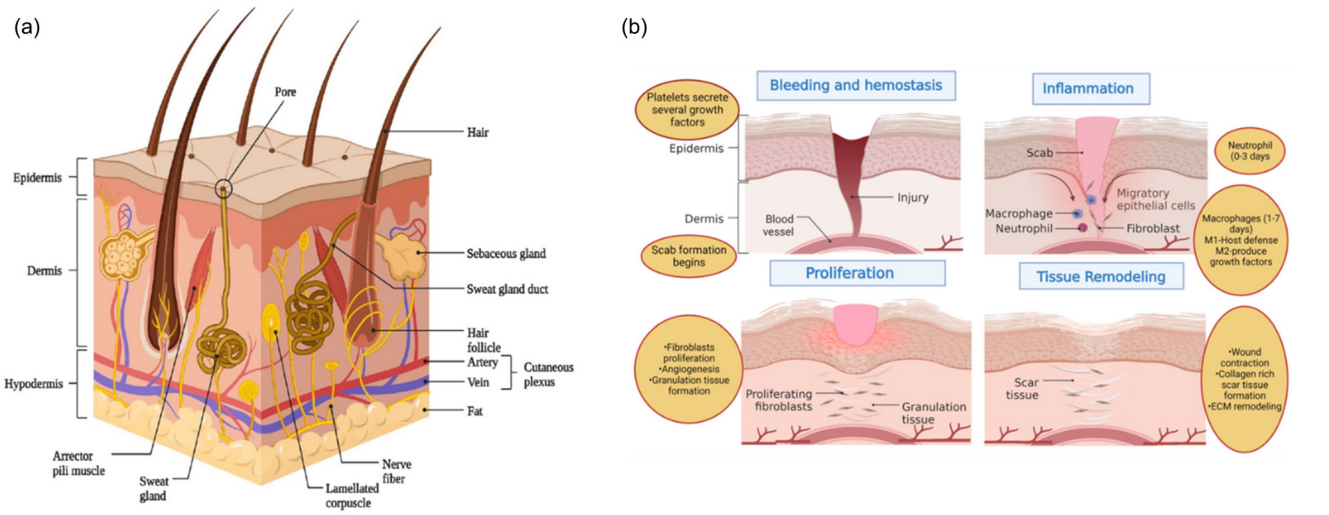

Fig. 5 (A) Anatomical illustration of skin structure. (B) Schematic representation of four steps for wound healing. Reproduced from ref. 1 under Creative Commons license.

factors such as Epidermal growth factor (EGF), Fibroblast growth factors (FGF), and Vascular endothelial growth factor (VEGF). Fibroblasts synthesize substantial amounts of type III collagen, proteoglycans, and fibronectin to form an extracellular matrix, which serves as a scaffold for cell migration and proliferation.[41] VEGF induces endothelial cells to migrate to the injury site and proliferate, forming new capillaries.[42] The capillaries, extracellular matrix, and keratinocytes in the wound form granulation tissue.

The healing process transitions into the remodelling stage approximately 2–3 weeks after injury, focusing on the formation of scar tissue. The granulation tissue, primarily composed of type III collagen with low elastic tension, is gradually replaced by type I collagen, which has higher tensile strength and is typical of normal skin tissue fibroblasts and collagenase continuously degrades and regenerates collagen in the granulation tissue, eventually producing a scar with mechanical strength comparable to normal skin.[43] Concurrently, excess capillaries and residual inflammatory cells formed during the repair process are gradually eliminated through apoptosis, culminating in the formation of scar tissue.[44]

In summary, ensuring proper neovascularization and regulating the immune microenvironment at the wound site is essential for rapid skin repair and scarless healing. Neovascularization is critical for providing nutrients; however, excessive vascularization can cause adverse effects, worsening tissue deterioration and leading to scar formation.[45] Additionally, inflammation should be kept under control: early anti-inflammatory therapy can prevent the accumulation of local inflammatory cells, inhibit the surge of inflammatory cytokines, and prevent further damage.[46] In this case, the anti-inflammatory M2 macrophages play a crucial role in inhibiting the excessive proliferation of fibroblasts and the over-deposition of the extracellular matrix during the later stages of wound healing.[47]

4.2. Wound models

External injuries, due to physical stimuli such as burns, radiation exposure, and blunt force are the most common skin damage. Different models are available to study wound healing and the *in vitro* wound scratch assay consisting of dermal fibroblasts and/or epidermal keratinocytes grown in 2D culture plates is the most basic. This method creates a cell-free region in a confluent cell monolayer using mechanical (pipette tip, cell scraper, metallic micro-indenter, and toothpick), optical (laser), electrical (electric cell–substrate impedance sensing), or thermal tools.[48]

The introduction of the 3R principle and growing concerns about animal welfare have prompted countries to take action to reduce and replace the use of animals, particularly in the pharmaceutical and cosmetic industries. In addition to numerous laboratory-developed epidermis tissues, commercially available epidermis models are constructed using primary keratinocytes and scaffolds (Fig. 6 from ref. 49). The primary purpose of using scaffold materials for *in vitro* biomimetic epidermal tissue reconstruction is to promote the adhesion of basal keratinocytes and facilitate the formation of the basal layer, thereby enhancing the performance of the reconstructed biomimetic epidermis tissues. A variety of scaffold materials have been investigated for this purpose, including fibrin, collagen, gelatin, glycosaminoglycans, and decellularized extracellular matrix. However, natural scaffold materials often suffer from insufficient mechanical properties and long gelation times. In contrast, synthetic scaffold materials exhibit more controllable mechanical and physicochemical properties. Examples are polyethylene glycol, polylactic acid, polycaprolactone, and poly lactic-*co*-glycolic acid, photocurable scaffold materials, such as gelatin-methacryloyl (GelMA), hyaluronic acid methacrylate, methacrylate silk fibroin, and poly (ethylene glycol) diacrylate (PEGDA).[49]

There are three main categories of 3D epidermis fabrication techniques: traditional tissue engineering techniques utilizing transwell chambers, epidermis-on-a-chip techniques based on microfluidics, and recently emerging tissue engineering techniques that employ 3D bioprinting (Fig. 6). The key distinctions among these three fabrication techniques lie in whether they involve fluid shear forces and how keratinocytes are seeded onto the polycarbonate membrane of the transwell chamber. Traditional tissue engineering techniques involve manually inoculating keratinocytes into a transwell chamber. The polycarbonate membrane of the transwell chamber promotes the adhesion of basal keratinocytes and the formation of the basal layer. By cultivating these epidermal cells at the air–liquid interface (ALI), an active, multi-layered epidermis resembling human skin is formed. The ALI facilitates the differentiation of epidermal cells and the formation of the stratum corneum.[49] Pumpless-guided gravity microfluidic systems nourish cultures with a membrane, promoting epidermal proliferation and differentiation. This process leads to the development of a functional epidermis with characteristics like the human epidermis. The epidermis-on-a-chip technique using a pump-driven dynamic microfluidic system cultivated human keratinocytes, forming an integrated epidermal structure similar to normal human skin. This dynamic culture improved the epidermis's barrier function. The microfluidic system with a multi-chamber design enhanced reproducibility.

3D bioprinting enables the creation of a heterogeneous skin model comprising both the dermis and epidermis using multiple printing heads equipped with various cell-laden bioinks which contain cells, proteins, growth factors, and other bioactive molecules to produce physiologically biomimetic skin models. The extrusion modules produce a fibroblast-populated dermis on a functional transwell system. Subsequently, keratinocytes are evenly distributed on it using the inkjet module. This straightforward biofabrication method creates mature skin models with a stratified epidermis similar in thickness and morphology to human epidermis. These biofabrication tools can be applied to engineer both healthy and diseased-skin models. After the formation of the full-thickness (FT) skin on the transwell system, wounding can be created by automatically inserting a needle at a constant depth and speed into the tissue.[48]

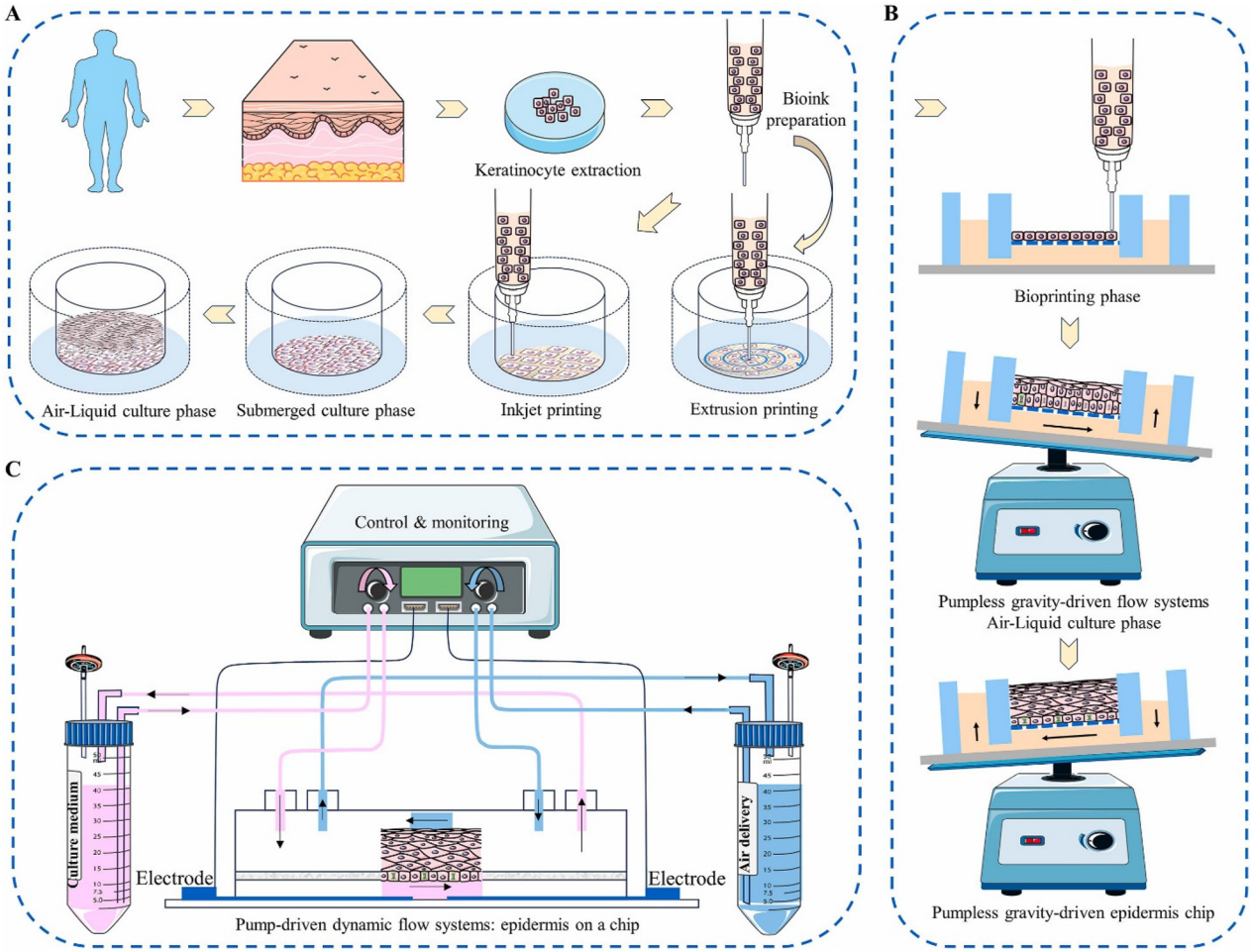

Fig. 6 (A) Illustration of various 3D epidermis creation methods. (A) 3D biomimetic epidermis tissue constructed using inkjet and extrusion printing techniques. (B) Epidermis-on-a-chip approach utilizing a pumpless, gravity-fed microfluidic system. (C) Epidermis-on-a-chip method employing a pump-activated dynamic microfluidic system. Reproduced with permission from ref. 49. Copyright 2024 The Authors. Published by Elsevier Ltd.

In vivo wound models facilitate the study of interactions between multiple cell populations during repair, allow the investigation of various elements of the healing process, and enable the selective depletion of specific genes to assess their impact on wound healing. These models also support the study of a functional immune system, the creation of multiple wounds within one animal, and the simulation of different wound-healing causes such as burns, surgery, and crushing injuries. The most used species for these studies are rats and mice, despite there are documented differences between rodent and human skin structure and physiology. Rats are a better choice than mice for wound healing studies due to the differences in skin characteristics. For example, mouse skin is thinner and has fewer layers of keratinocytes compared to rat skin, leading to faster wound healing.[50]

While rats, mice, and rabbits are common in experimental dermatological studies, pig skin is considered the most anatomically and physiologically similar to human skin, though more expensive and prone to infections. Excisional wounds are among the most used wound healing models and are considered to resemble acute clinical wounds, which require healing by secondary closure where the skin edges are not sutured together. Other models include burn or diabetic wounds. Burn wound healing models can be created either by water scalding (hot water) or thermal damage (hot metal plate). Two of the most frequently used models to simulate impaired healing processes are related to diabetes and nutritional conditions commonly observed in wound care clinics. Diabetic animal models can be created through chemical or dietary induction, surgical manipulations, or systemic mutations such as diabetes/diabetes (db/db) and obese/obese (ob/ob) mice. Chemically induced type 1 diabetes is usually achieved by administering drugs like alloxan or streptozotocin. On the other hand, genetic models allow the investigation of the natural mechanisms of diabetes without the potential side effects of chemical treatments. Other systemic factors, such as metabolic diseases (including metabolic syndrome and obesity), increase the concentration of ROS and disrupt the wound healing process and can be used to analyze delayed wound repair.[50]

5. Current skin treatments based on MXenes

Despite MXenes being a relatively recently synthesized material, their applications centered on wound healing and skin patches have been numerous over 13 years, with more than ten patents on wound dressing published.[51]

Given the multiple biological activities and stimulus responsiveness of MXenes, many studies have focused on different diseases, such as diabetic chronic wounds or cancer treatment. The tables in the following sections summarize the antibacterial, tissue regeneration, and therapeutic applications of MXenes-based materials together with their specific sensing capacity.

5.1. Wound healing

Effective wound healing patches should possess several critical requirements, including strong antibacterial properties to prevent infection, the ability to promote neovascularization to enhance blood supply and tissue regeneration, and the synergistic anti-inflammatory effects to reduce scar tissue formation. Additionally, they should be biocompatible, ensuring no adverse reactions when in contact with the skin, and capable of maintaining a moist environment to facilitate healing. Durability, flexibility to conform to wound contours, and the ability to deliver therapeutic agents in a controlled manner are also essential for optimal performance.[1]

Two fundamental features of MXenes are used in these applications: the NIR adsorption that induces eventual drug release or produces PTT effects on bacteria/cancer cells/immune cells, or the intrinsic MXene-polymer properties, such as conductivity. Indeed, electrical conductivity improves cellular repairing properties or can improve antibacterial effects with or without the combination of NIR effects. Furthermore, electrical conductivity provides sensor properties of the patches as described in section 5.[52]

In Table 1, the wound healing patches developed for general purposes are reported. The polymeric structure of the patches is usually made of polyvinyl alcohol, acrylamide-based hydrogels, chitosan, sodium alginate and hyaluronic acid, among many others. Polydopamine (PDA) is also often added to hydrogels for its photothermal conversion capabilities and strong adhesive properties, which can be combined with various organic and inorganic molecules. Furthermore, PDA-based hydrogels and scaffolds can effectively mimic the extracellular matrix, facilitating cell attachment and growth.

5.1.1. Antibacterial effects in MXene wound dressing. Antibacterial effects can be achieved by combining MXenes with amoxicillin,[53] silver nanoparticles,[54,84–87] ciprofloxacin,[55] antimicrobial peptides,[56] natural antibacterial compounds such as chitosan[61–63] or ions such as copper whose release can be spontaneous or obtained upon NIR irradiation.[57,58,65,81,88]

Among many polymers, chitosan, an exoskeleton biopolymer derived from chitin, has garnered significant attention for its antibacterial properties, which include electrostatic interaction and physical damage of bacterial membranes and metal chelation.[89] Chitosan-MXenes have been used to embed fabric in super-hydrophilic $Ti_3C_2T_x$-PDA-decorated non-woven fabric;[61] chitosan-Ti_3C_2-and positively charged cobalt tungsten nanocomposites have been used to reduce inflammation during the initial stages of wound healing process while keeping good antibacterial effects[62] and in burn wound healing.[63] In addition, chitosan and MXenes have also been combined to obtain cryogels[64] and sponges[65] with hemostatic and wound healing properties.

As previously discussed, antibacterial effects of MXenes can be obtained by direct contact with the nanomaterial or, more effectively, by a light-triggered production of ROS or local increase in the temperature, *i.e.*, by PDT or PTT.[67–69] In most of the papers, a power density comprised between 0.2 and 1.5 W cm^{-2} for an exposure time of up to 10 (rarely up to 15) minutes and a wavelength of 808 nm has been used. An exception is the work of Su *et al.*, which is based on a therapy using a 980 nm laser with multiple treatments,[58] which has been demonstrated to promote ROS generation.[90]

Interestingly, besides exogenous ROS generated by PDT/PTT, Yang *et al.* designed a Ti_3C_2 MXene/MoS_2-based strategy to attack the intracellular oxidative stress protection mechanisms of bacteria. The two-step mechanism is based on Mo^{4+} peroxidase (POD)-like activity, which converts hydrogen peroxide to $^{\bullet}OH$ and is oxidized to Mo^{6+}. In turn, Mo^{6+} possesses glutathione oxidase-like activity, which can oxidize glutathione (GSH) to glutathione disulfide (GSSG) and be again converted to Mo^{4+}. This cyclic Mo^{4+}/Mo^{6+} redox pair can significantly reduce GSH and create a ROS hurricane in bacteria when combined with extracellular PDT-generated ROS. Furthermore, to avoid the impact of ROS on healthy tissues fibroblast growth factor-21 (FGF21) has been loaded in the patch to reduce inflammation and accelerate fibroblast migration and wound repair *in vivo* Fig. 7 from ref. 66.

Kang and colleagues also achieved multiple effects exploiting PTT and ROS generation from the wound dressing, using quaternary ammonium-modified chitosan-sulfonic betaine acrylamide hydrogel loaded with Ti_3C_2/Fe nanosheets. The nanosheets demonstrated both catalase (CAT)-like and POD-like activities, with MXene's high conductivity enhancing the electron transfer rate and facilitating the conversion between Fe(II) and Fe(III). The POD-like activity, combined with PTT, provided potent antibacterial effects, while the CAT-like activity generated oxygen and alleviated tissue stress. *In vivo* experiments confirmed that the hydrogel significantly promoted burn wound healing by supporting granulation tissue regeneration, epithelial layer formation, and collagen deposition. The zwitterionic sulfonate betaine acrylamide component exhibited excellent antifouling properties, preventing protein adsorption, bacterial adhesion, and subsequent wound infection.[63]

Copper ions have been proven to possess broad-spectrum antibacterial efficacy, effectively disrupting bacterial cell membranes, generating ROS, and interfering with essential microbial enzymes and DNA replication. In the work of Liu and colleagues, copper ions are released in response to NIR

Table 1 *In vivo* tested wound healing patches based on MXenes

Composition	Antibacterial mechanism/ tested species	Tissue Regeneration/therapeutic effects	Animal model	Triggering mechanism/ sensor	Ref.
$Ti_3C_2T_x$ amoxicillin-polyvinyl alcohol (PVA) nanofibrous membrane	Amoxicillin/PTT, *S. aureus*, *E. coli*	Hemocompatible and cytocompatible	Infected BALB/c mice (*S. aureus*)	NIR-mediated release	53
$Ti_3C_2T_x$, silver polycarboxybetaine acrylamide hydrogel	Silver/PTT, *S. aureus*, *E. coli*	Excellent antibacterial inhibition and thick granulation tissue formation	Infected BALB/c mice (*S. aureus*)	NIR-mediated release	54
Ti_3C_2 ciprofloxacin sodium alginate hydrogel	Ciprofloxacin *S. aureus*, *E. coli*	Enhanced collagen deposition and angiogenic activation	BALB/c-nu mice	NIR-mediated release	55
$Ti_3C_2T_x$, GelMa polypeptide Os, hydrogel GelMa, GelMa/Os, GelMa/$Ti_3C_2T_x$, GelMa/Os/$Ti_3C_2T_x$ composites	Antimicrobial peptides, *S. aureus*, *E. coli*	Antibacterial efficacy, mechanical support, and promotion of tissue formation	Adult rats	—	56
Ti_3C_2 copper hyaluronic acid hydrogel	Copper/PTT, *S. aureus*, *E. coli*	Increased epithelialization, reduction of inflammation, enhanced collagen deposition, angiogenesis and regenerative tissue	C57BL/6 mice	NIR-mediated release	57
$Ti_3C_2T_x$, CuS, PVA, PDA, hydrogel	Copper/PTT, *S. aureus*, *E. coli*	Good biocompatibility, reduced inflammatory state, improved angiogenesis and collagen deposition	Infected mice (*S. aureus*)	NIR-mediated release	58
Ti_3C_2, Ag_2PO_4, PCL, PDA, nanofibrous membrane	*E. coli*, *S. aureus*	Reduced inflammation, and improved collagen deposition	Infected (*S. aureus*) Kunming mice	NIR-mediated release of silver ions	59
$Ti_3C_2T_x$, Ag_2S, PLGA electrospun membrane	*E. coli* (*in vitro*), *S. aureus*	Transformation of the chronic wound into a regenerative one by eliminating bacteria, stopping bleeding, enhancing epithelialization and collagen deposition, and promoting angiogenesis	*S. aureus* infected male Kunming mice	NIR Mediated PTT and ROS generation during PLGA degradation	60
$Ti_3C_2T_x$, PDA, chitosan, non-woven fabric	Chitosan, *S. aureus*, *E. coli*	Improved wound healing and hemostatic ability, reduced inflammation	Rats	—	61
Ti_3C_2, chitosan, cobalt tungsten layered doubled hydroxide composite	Chitosan, *S. aureus*, *E. coli*	Promoted fibroblast growth, granulation tissue formation, deposition of collagen, re-epithelialisation of skin wounds and angiogenesis. Inhibition of inflammatory response	Wistar rats	—	62
Ti_3C_2/Fe, chitosan-sulfonic betaine acrylamide hydrogel	PTT chitosan nanozymes, *S. aureus*, *E. coli*	Epidermal growth, collagen deposition, angiogenesis, and wound healing enhanced. Hypoxia is alleviated.	Burn wounds in rats	NIR PTT	63
$Ti_3C_2T_x$, copper, chitosan, *N*-hydroxyethyl, acrylamide cryogel	PTT chitosan copper, *S. aureus*, *E. coli*	Hemostatic histo- and hemocompatible, pro-angiogenic and anti- inflammatory	Mice BALB/c, white and C57bl/6, black	NIR PTT	64
$Ti_3C_2T_x$, copper, chitosan sponge	PTT copper, *S. aureus*, *E. coli*	Great histocompatibility, angiogenesis without inflammatory reaction. After 10 days, a relatively Epidermal layer more vascularized with hair follicles	Mice	NIR-mediated release PTT	65
MoS_2 Ti_3C_2, PDA, fibroblast growth factor-21 (FGF21) bioheterojunctions	Intracellular and extracellular ROS stress *S. aureus* and *E. coli*	FGF-21 accelerated self-repair *via* enhanced angiogenesis and cell migration, and by regulating inflammation and oxidative stress	Infected BALB/c mice (*S. aureus*)	NIR-mediated release PTT	66
$Ti_3C_2T_x$ – gold nanoparticles chitin sponge	PTT, *E. coli*, *S. aureus*	Gold nanoparticles promote the migration of keratinocytes and fibroblasts and improve haemostatic ability	Infected mice (*S. aureus*)	PTT	67
Ti_3C_2, PVA hydrogel	PTT, *E. coli*, *S. aureus*	High toughness and anisotropy properties due to muscle-like assembly	Infected mice (*S. aureus*)	PTT	68
$Ti_3C_2T_x$, polyaniline (PANI)-PVA	PTT, *E. coli*, *S. aureus*, (*in vitro*)	Promote proliferation and enhance the migration of cells by electrical stimulation. Accelerated wound healing by fostering angiogenesis and collagen deposition	Mice	NIR antibacterial effect *in vitro*	69

Table 1 *(Contd.)*

Composition	Antibacterial mechanism/ tested species	Tissue Regeneration/therapeutic effects	Animal model	Triggering mechanism/ sensor	Ref.
$Ti_3C_2T_x$, alginate dialdehyde gelatin	—	*In vitro* promotion of cell growth	—	—	70
$Ti_3C_2T_x$ regenerated bacterial cellulose	—	Good mechanical properties, flexibility, biodegradability, and high water-uptake capacity. Wound healing performance higher than commercial film	Sprague Dawley (SD) rats	Electrical stimulation	71
$Ti_3C_2T_x$, PCL-gelatin electrospun membranes	*E. coli*, *S. aureus*	Enhanced vascularization due to endogenous electrical stimulation	SD rats	Electrical stimulation (*in vitro*)	72
$Ti_3C_2T_x$, chitosan, PVA, AgCu-pyridine-3,5-dicarboxylic acid hydrogels	Electrical stimulation *E. coli*, *S. aureus*	Good mechanical properties, flexibility and biodegradability. Wound healing performance higher than commercial film	BALB/c infected mice (*S. aureus*)	Electrical stimulation	73
$Ti_3C_2T_x$, acrylic acid, ionic gel	NIR effects on *E. coli* and *S. Aureus*	Decreased margins of the wound with more collagen deposition, lower expression of TNF-α and upregulation of FGF-2	*S. aureus* infected mice	NIR antibacterial effect + Electrical stimulation	74
$Ti_3C_2T_x$, polyvinylidene fluoride, electrospun fibers	—	Skin wound healing and oral mucosa repair. Improved deposition of collagen, formation of granulation tissue, angiogenesis and wound healing	SD rats	Electrical stimulation	75
Ti_3C_2, adenosine-3-(acrylamido)phenylboronic acid- d polyethylene glycol diacrylate hydrogel integrated, microneedle patch	—	Skin wound healing, proangiogenic effect of adenosine	SD rats	NIR-mediated release	76
Mxene (acetylsalicylic acid deferoxamine mesylate), poly(L-lactide) nanofibers hydrogel	—	neo angiogenesis and anti-inflammatory effects of acetylsalicylic acid	BALB/c mice	NIR-mediated release	77
$Ti_3C_2T_x$, gelatin, poly(ethylene glycol)diacrylate and *N*,*N*′-methylenebis(acrylamide)	—	Shape memory. Wound healing with more complete skin-appendage structures	C57 mice	NIR-mediated wound repair	78
$Ti_3C_2T_x$ vitamin E, poly(acrylamide-*co*-acrylonitrile-*co*-vinylimidazole-*co*-bis(2-methacryloyl))oxyethyl disulfide copolymer, nanobelt fibers	—	Neo angiogenesis due to vitamin E	Kunming mice	NIR-mediated release	79
Ti_3C_2 VEGF, diallyl trisulfide, mesoporous silica nanoparticles and dopamine-hyaluronic acid, PLGA hydrogels	—	Scarless wound healing, neo angiogenesis and anti-inflammatory effects (release of VEGF and diallyl trisulfide)	BALB/c mice	NIR-mediated release of drug	80
$Ti_3C_2T_x$, copper sulfide, VEGFA-mimicking peptides, bioheterojunctions	PDT/PTT, *E. coli*, *S. aureus*	Neo angiogenesis and anti-inflammatory effects	Ischemic infected mice (*S. aureus*)	NIR-mediated release of drug PDT/PTT	81
Ti_3C_2, 3D-printed *N*-isopropylacrylamide alginate scaffold	—	Large skin flap angiogenesis and wound repair	C57BL/6 mice	NIR-mediated release of VEGF	82
Ti_3C_2, IL17 antibodies, hyaluronic acid	—	Psoriasis treatment due to the release of antibodies. IL-17, IL-6, IL-22, IL-23a and IFN-γ decreased, resulting in the alleviation of inflammation and epidermal proliferation	BALB/c mice	NIR-mediated release of antibodies	83

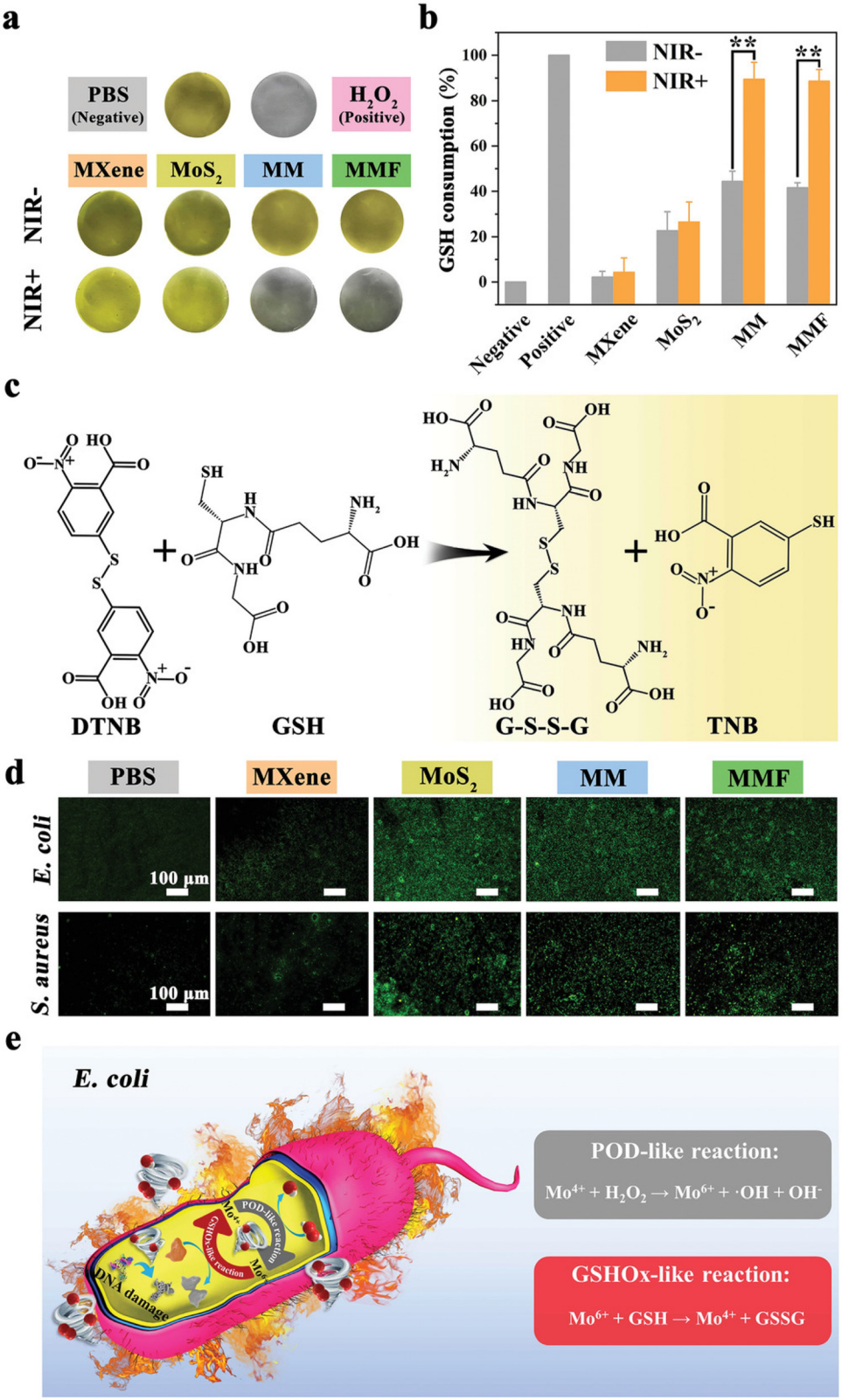

Fig. 7 GSH mechanism involved for evaluating the antibacterial effect of Ti_3C_2 MXene/MoS_2 2D Bio-Heterojunctions. (a) Shows the changes in colour of GSH in different media. (b) Illustrates the percentage of GSH consumption with and without NIR irradiation applied to different materials. (c) Reaction of GSH with DTNB, giving GSSG and TNB as final products. (d) Images by fluorescence microscopy describing intracellular ROS production in different samples. (e) POD-like reaction compared to GSH-like reaction applied for *E. coli*. Reproduced with permission from ref. 66. Copyright 2021 Wiley-VCH GmbH.

stimulus from Ti_3C_2 hyaluronic acid hydrogel with photothermal antibacterial effects, and concurrently ROS scavenging and angiogenesis promotion.[57] Similarly, PVA/PDA/Ti_3C_2/CuS hydrogel can exhibit both PTT and PDT activated by NIR with copper-sustained antimicrobial capacity.[58]

Since the bactericidal effect of phototherapy can be time-limited, Yang and colleagues created an antibacterial fibrous membrane composed of electrospun polycaprolactone scaffolds and PDA-coated Ti_3C_2 Ag_2PO_4 bioheterojunctions (MX@AgP). Under NIR illumination, the MX@AgP nanoparticles in the nanofibrous membranes exert a strong bactericidal effect and release Ag^+ ions, preventing bacteria from multiplying. When NIR light is removed, PDA reduces Ag^+ ions to Ag nanoparticles, enabling the self-rechargeability of Ag^+ ions for subsequent phototherapy (Fig. 8 from ref. 59).

In vivo results demonstrate that photoactivated nanofibrous membranes can regenerate infected wounds by killing bacteria, stopping bleeding, increasing epithelialization, and inducing collagen deposition on the wound bed, as well as promoting angiogenesis.[59]

The same authors conceived an infection microenvironment-activated nanocatalytic composed of electrospun poly (lactide-*co*-glycolide) (PLGA) scaffolds, $Ti_3C_2T_x/Ag_2S$ bio-heterojunctions and lactate oxidase (LOx). This system works by the PLGA membranes gradually degrading into lactate, which LOx then converts into pyruvic acid hydrogen peroxide (H_2O_2). Then under NIR light $Ti_3C_2T_x/Ag_2S$ bio-heterojunctions catalyze the H_2O_2 to produce hydroxyl radicals ($^{\bullet}OH$) *via* Fenton-like reactions, achieving rapid and synergistic sterilization in combination with PTT. *In vivo* studies show that these membranes effectively transform chronic wounds into a regenerative state by killing bacteria, stopping bleeding, promoting epithelialization, and enhancing collagen deposition and angiogenesis.[60]

5.1.2. NIR-mediated drug release and electrical stimulation of patches. A previously discussed NIR responsiveness of MXenes is largely exploited in this field of research. The infrared stimulus can be exploited to confer shape memory and prohealing properties to hydrogel[78] or release growth factors, as previously described for FGF21.[66] MXene nanosheets in polyacrylonitrile/polyvinylpyrrolidone nanobelts together with a thermosensitive PAAV-coating layer can release vitamin E, which positively impacts *in vivo* healing and angiogenesis in the wound.[79] Also, adenosine can improve neovascularization when released from Ti_3C_2 microneedle patch[76] or hepatic growth factor (hGF) can improve migration of cells towards the wound *via* the c-Met-mediated signalling after NIR irradiation of MXene-agarose patch.[91]

Electrical stimulation (ES) of the patch can be exploited in multiple phases during wound repair. In the early phase of inflammation, ES induces cytokine production and recruitment of immune cells. During the inflammation phase, a certain degree of improvement of antibacterial effects can be achieved by ES; the edema that might form in the wound can be decreased, and the fibroblasts, endothelial cells, and epithelial cells, are stimulated to migrate in the damaged tissue. Finally, scar tissue thickness can be diminished by ES.[52]

Examples of uses of ES to accelerate skin repair by exploiting MXenes electrical conductivity include alginate dialdehyde-gelatin,[70] bacterial-derived cellulose and $Ti_3C_2T_x$[71] or electrospun PCL-gelatin-6 $Ti_3C_2T_x$ membranes.[72] In the latter, a double tissue repair-antibacterial effect was achieved with a significant promotion of wound healing compared to the commercial Tegaderm patch. Also, $Ti_3C_2T_x$ hydrogels composed of chitosan and PVA modulated cell behavior and provided ES antimicrobial capacity under ES at 1 V with good biocompatibility and wound healing after 14 days of treatment.[73] Feng and colleagues demonstrated that external ES of skin wounds

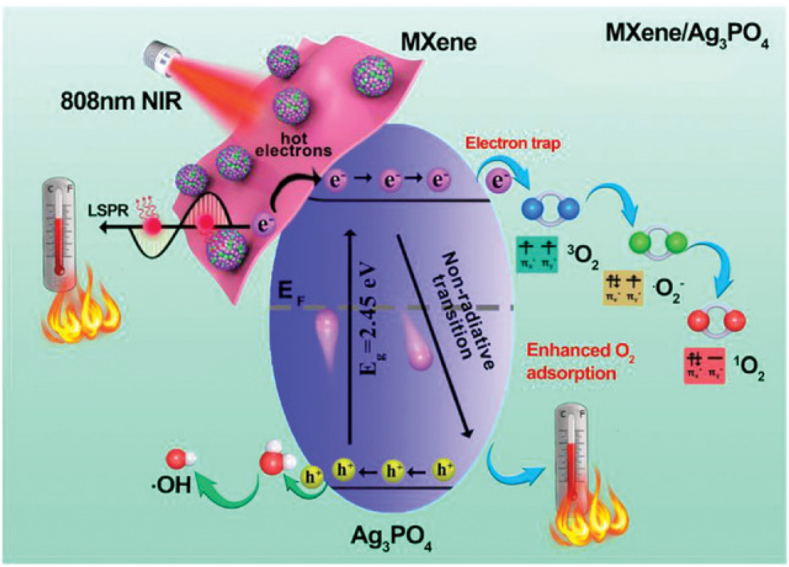

Fig. 8 Illustrates the electron transition process initiated by NIR irradiation of MXene/Ag_3PO_4 material. Adapted with permission from ref. 59. Copyright 2022 Wiley-VCH GmbH.

treated with $Ti_3C_2T_x$ polyvinylidene fluoride electrospun fibers, allows the repairing of skin or oral defects, however even the physiological current is sufficient for oral mucosa healing with the same treatment, due to the not significant differences in gel with or without ES in the latter case.[75]

Concerning the combination of NIR and ES, a $Ti_3C_2T_x$ acid acrylic ionic gel enhanced skin wound healing due to combined NIR antibacterial effects on *E. coli* and *S. aureus* and increased cell migration due to ES in infected mice.[74] In this study, while the inflammation and necrotic tissue were evident in the wounds in the control, only the combined ES and PTT, decreased the margins of the wound with enhanced collagen deposition, lower expression of TNF-α and upregulation of FGF-2.

5.1.3. Proangiogenesis and antiinflammatory effects. Angiogenesis is modulated by several signalling molecules, with vascular endothelial growth factor A (VEGFA) representing the central signal to stabilize new vessels and control their permeability by binding to VEGF receptors. Several ions can elevate neovascularization by upregulating VEGFA expression and stabilizing hypoxic inducing factors 1α (HIF-1α) expression (endogenous pathway); on the other end, supply of VEGFA or biomimetic peptides – known as VEGFA-mimicking peptides (VMPs) – can activate receptors *via* exogenous pathway.[81] In recent work, Li and colleagues exploited the double activation of both VEGF pathways for ischemic wound healing using MXene, copper sulfide (CuS), and VMP obtaining vascularization capabilities thanks to copper-facilitated VEGFA secretion from fibroblasts, endothelial cell proliferation and migration, leading to increased angiogenic effects (Fig. 9). Furthermore, PTT and PDT bac-

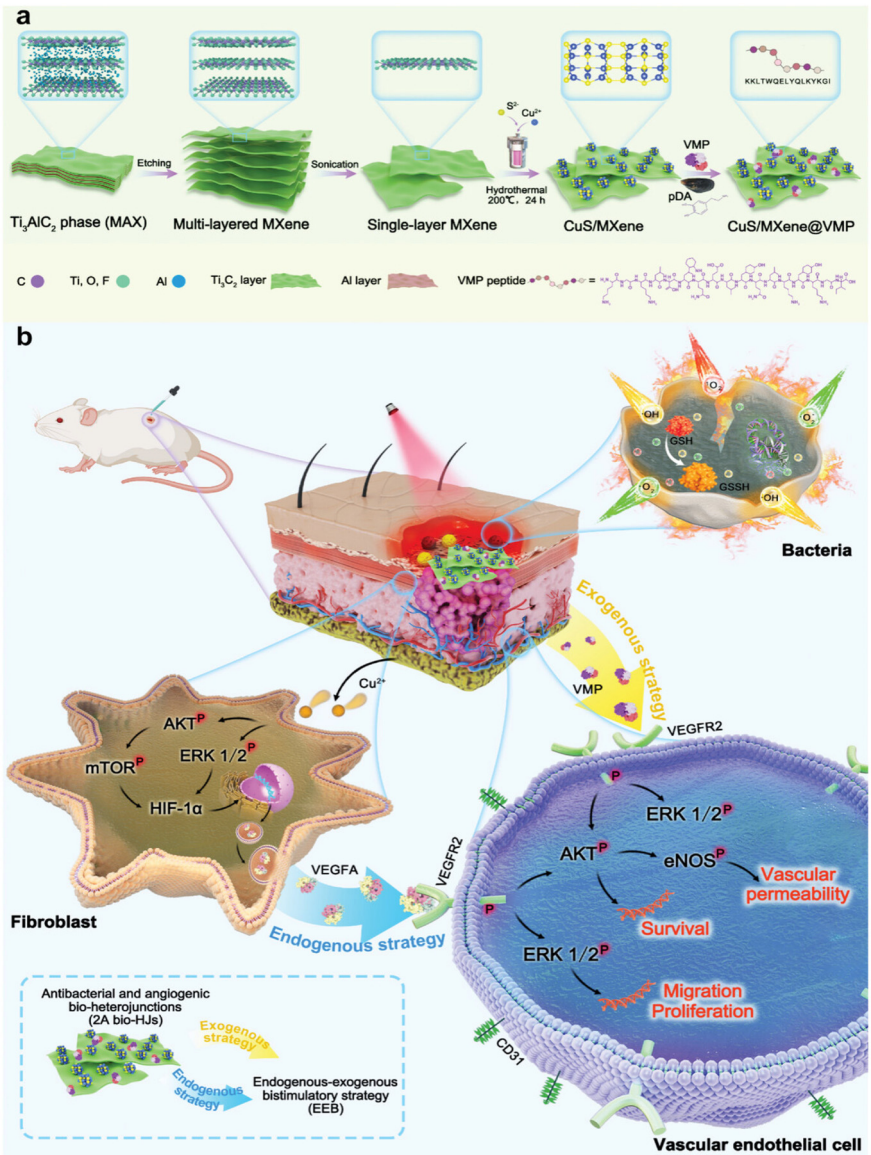

Fig. 9 Synthesis of Cu/MX@VMP 2° bio-HJ system for antibacterial treatment (a) and wound healing (b). Reproduced with permission from ref. 81. Copyright 2023 Wiley-VCH GmbH.

tericidal activities have been observed in an *in vivo* model of ischemic infected wound.[81]

VEGF release has been also exploited for large-scale defects restoration *via* skin flap technology based on 3D-printed Ti_3C_2 *N*-isopropylacrylamide (NIPAM)-alginate scaffold. Skin flaps are used in large trauma, tumor, or congenital defects but suffer from necrosis due to poor blood supply and this paper is one of the few examples of 3D printed MXene scaffold. With the NIR-mediated increase in temperature, the VEGF release has been controlled using reversible shrinkage/swelling properties and obtaining low inflammation and wound healing *in vivo*.[82]

Electrospun PLGA fibers loaded with Ti_3C_2 nanosheets and VEGF-silica nanoparticles spin-coated with dopamine-hyaluronic acid hydrogel were used to obtain an immune-controlling band-aid that avoided excessive immune stimulation and scar formation. The NIR irradiation at 808 nm induced the release of VEGF, while the hydrogel continuously produces diallyl trisulfide and H_2S promoting polarization of macrophages towards the anti-inflammatory M2 phenotype. The macrophagic release of anti-inflammatory cytokines regulates the immune microenvironment at the wound site while the scar is kept vascularized *via* the VEGF-controlled release.[80]

Neovascularization and synergistic anti-inflammatory effects have also been obtained when combining deferoxamine mesylate and acetylsalicylic acid with MXene NIR responsive electrospun Poly(L-lactide) nanofibers.[77]

Anti-inflammatory effects are essential for the treatment of psoriasis disease when the hyperproliferation of keratinocytes and infiltration of inflammatory cells into the epidermis induce skin thickening. Photo-thermally dissolvable hyaluronic acid microneedle patch has been demonstrated to be useful for the release of IL-17 mAbs thanks to the NIR activation of Ti_3C_2 MXenes in the hydrogel.[83] The combination of patch loading with MXenes and IL-17 mAbs irradiating by NIR showed a decrease of inflammatory cytokines such as IL-17, IL-6, IL-22, IL-23a, and IFN-γ. This result demonstrated that the patch loaded with MXenes activated by NIR can inhibit epidermal proliferation and alleviate psoriatic skin inflammation. Interestingly, MXene combined with multi-walled carbon nanotubes sensors can also be exploited for psoriasis screening of the metabolic fingerprint with laser desorption/ionization-mass spectrometry.[92]

5.2. Chronic and diabetic wounds

Currently, approximately 537 million people worldwide are living with diabetes, and around 25% of these individuals eventually require surgical amputation.[93] Due to their unique microenvironment, diabetic wounds are more prone to infection and are challenging to heal. The four phases of normal wound healing can be disrupted or delayed in diabetic patients (Fig. 10) since biochemical disorders including hyperglycaemia, dyslipidaemia, and insulin resistance, lead to tissue damage, excessive inflammation, and destruction of tissue.

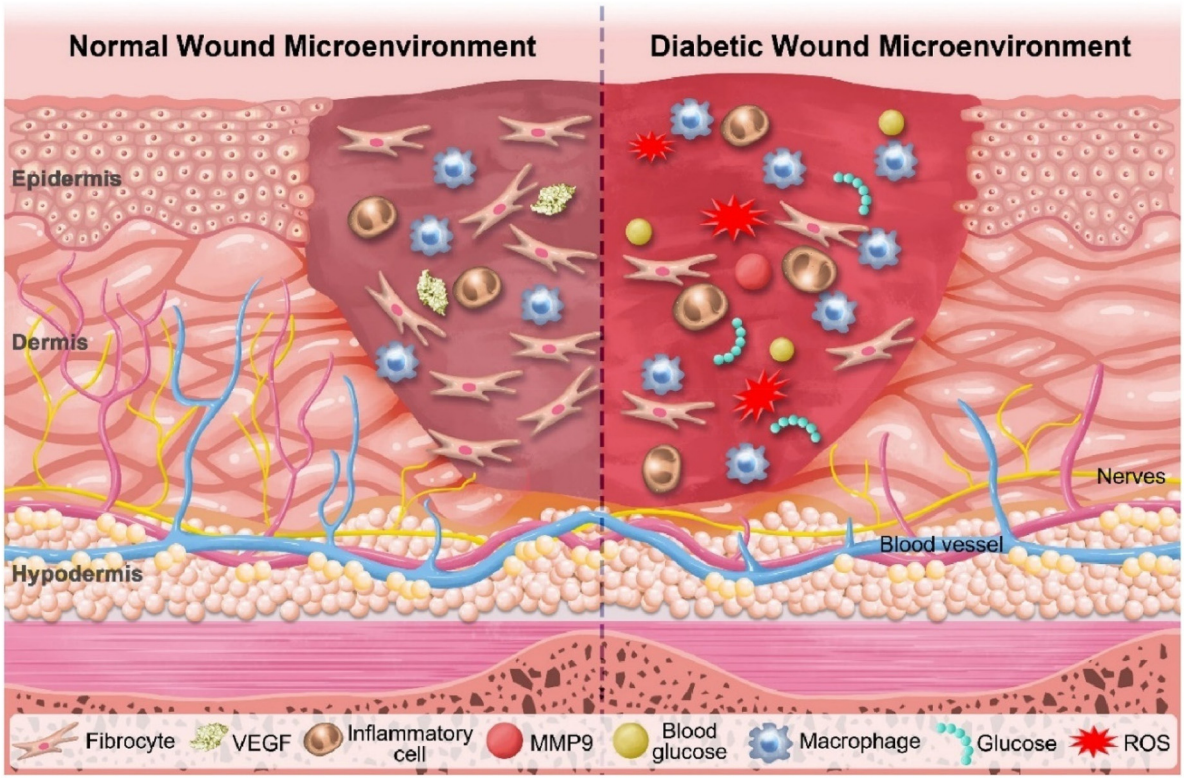

Fig. 10 Microenvironments in normal wound (left) and diabetic wound (right). Reproduced with permission from ref. 95. Copyright 2022 The Authors. Published by Elsevier Ltd.

The abnormal function of immune cells hampers the suppression of inflammation, significantly increasing the susceptibility to infection. Once a chronic wound becomes infected, persistent inflammation maintains a cycle of infection, inflammation, and inadequate repair. Furthermore, studies indicate that excessive oxidative stress and reduced antioxidant capacity are key factors in the non-healing of diabetic wounds. The balance between pro-angiogenic and anti-angiogenic factors, crucial for maintaining blood vessel perfusion to deliver nutrients and oxygen, is disrupted. This results in reduced angiogenesis and nerve cell dysfunction. In addition to hyperglycaemia, a reduction in several neuropeptides associated with neuropathy impairs vasodilation and angiogenesis, leading to ischemia.[94]

Unlike normal wounds, diabetic wound infections often involve multiple drug-resistant bacterial species. Increasing evidence points to microbiome dysbiosis in the skin of diabetics, with higher colonization of *S. aureus* and *S. epidermidis*. Bacteria such as Staphylococcus and Streptococcus produce proteolytic factors that disrupt the skin barrier, with *S. aureus* potentially spreading infections to the bone and bloodstream. Unfortunately, systemic antibiotics have limited effectiveness in chronic wound sites, especially when a bacterial biofilm is present.[96]

In Table 2 the specific MXenes-based solutions for diabetic wounds are summarized.

Multifunctional scaffolds with self-healing and tissue adhesive features, electrical conductivity, antibacterial activity and rapid hemostatic capability are represented by $Ti_3C_2T_x$ PDA hyaluronic acid scaffolds, that also have anti-inflammation effects, promoting cell proliferation, and angiogenesis, stimulating granulation tissue formation even in MRSA infected mice.[97] Also based on hyaluronic acid, the microneedle patch containing Ti_3C_2 can eradicate MRSA infection *in vivo* using photothermal treatment.[98]

The active ingredient extracted from Salvia miltiorrhiza cryptotanshinone has both anti-inflammatory/antioxidant effects and antibiofilm effects and has been demonstrated to be extremely effective on MRSA-infected mice when combined with the PTT with Ti_3C_2 PDA hydrogels.[99]

To reduce the contribution of inflammatory response an injectable self-healing alginate hydrogel containing $Ti_3C_2T_x$ has been combined with antioxidant ultrasmall ceria CeO_2 and applied to treat MRSA-infected skin in rats using Pluronic F127 as a crosslinker. The scaffold possesses multifunctional properties including fast haemostatic capacity improved migration and cell proliferation when electrically stimulated (*in vitro* test) and re-epithelialization compared to commercially available Tegaderm 3M films and Aquacel Ag.[100] Genetic analysis of CeO_2/Nb_2C photothermal effects on ampicillin-resistant *E. coli* and *S. aureus* (MRSA) in diabetic mice displayed dysfunction in energy metabolism, cell morphology, and oxidative stress systems of photothermally treated bacteria.[101]

Also based on alginate, poly(*N*-isopropyl acrylamide)-alginate Ti_3C_2-wrapped $Fe_3O_4@SiO_2$ magnetic nanoparticles can

Table 2 *In vivo* wound healing for chronic and diabetic infections

Composition	Antibacterial mechanism/ tested species	Tissue Regeneration/therapeutic effects/other	*In vivo* model	Triggering mechanism/sensor	Ref.
$Ti_3C_2T_x$, poly(glycerol-ethylenimine), PDA, oxidized hyaluronic acid	*E. coli*, *S. aureus* and methicillin-resistant *S. aureus* (*MRSA*)	Wound healing, anti-inflammatory and haemostatic effects	MRSA-infected mice	—	97
Ti_3C_2, hyaluronic acid	*E. coli*, *S. aureus MRSA*	Controlled ROS effects, re-epithelialization, increased collagen deposition, and angiogenesis and inhibition of pro-inflammatory factors	MRSA-infected SD rats	NIR-mediated PTT	98
$Ti_3C_2T_x$ cryptotanshinone, PDA	Cryptotanshinone + NIR, Ampicillin resistant *E. coli*, *S. aureus MRSA*	PDA has ROS scavenging effects to promote healing	MRSA- infected mice	NIR-mediated PTT	99
$Ti_3C_2T_x$, CeO_2, polyethylenimine oxidized sodium alginate injectable hydrogel	*E. coli*, *S. aureus*, *S. aureus*, *MRSA*	Injectable self-healing behavior, efficient anti-inflammatory, antibacterial, and antioxidative properties, conductive and fast hemostatic capacity. Promoted fibroblasts migration, proliferation, granulation tissue formation, collagen deposition, re-epithelialization	MRSA-infected rats	—	100
Nb_2C, CeO_2 nanocomposite	Ampicillin-resistant, *E. coli*, *S. aureus MRSA*	Improved wound healing, antibacterial and haemostatic activity.	MRSA-infected diabetic mice	NIR-mediated PTT	101
Ti_3C_2-wrapped $Fe_3O_4@SiO_2$ magnetic nanoparticles poly(*N*-isopropyl acrylamide)-alginate hydrogel	*S. aureus*, *E. coli*	Healing of subcutaneous and epidermal wound s	Diabetic SD rats	NIR-mediated release of silver nanoparticles	86
Ti_3C_2 hyaluronic acid, PDA hydrogel	*E. coli*, *S. aureus*	Anti-inflammation effects	*S. aureus* infected diabetic rats	NIR-mediated PTT	102
Ti_3C_2, acrylic acid methacrylamide dopamine hydrogels	*E. coli*, *S. epidermidis*	Healing of full thickness excisional wounds, antioxidant activity	Diabetic mice	NIR-mediated PTT	103

release silver ions due to thermal shrinkage after NIR irradiation and induce the repair of the wound in diabetic rats.[86] *In vivo* studies revealed that the system irradiated with NIR enhanced wound healing, antibacterial activity and angiogenesis. Immunohistochemistry analysis showed an increase of CD163 markers in hydrogel loaded with silver nanoparticles and irradiated with NIR, compared with controls and non-irradiated hydrogel. CD163 positivity demonstrated an increase in the M2 macrophages population in the system which produces anti-inflammatory cytokines and promotes tissue regeneration.

Hyaluronic acid PDA-coated Ti_3C_2 nanosheets have been developed through the oxidative coupling of catechol groups catalyzed by the H_2O_2/HbO_2 system.[102] The DA enhances HA tissue adhesion, which helps to prevent bacterial invasion, maintain moisture, and achieve haemostasis. Additionally, the DA molecules impart anti-inflammatory properties to the HA-DA-based hydrogels by regulating macrophage polarization, promoting skin reconstruction. HbO_2 serves dual functions: it acts as an HRP-like enzyme to catalyze hydrogel formation and as an oxygen carrier to control oxygen release, stimulated by heat from NIR irradiation. Ti_3C_2 MXene nanosheets convert NIR into heat, kill bacteria, and scavenge ROS to maintain intracellular redox balance and alleviate oxidative stress.

This injectable hydrogel accelerates the healing of infected diabetic wounds by supplying oxygen, scavenging ROS, eradicating bacteria, and promoting angiogenesis and M2 macrophage-polarization.[102]

Similarly, sponge-like macro-porous acrylic acid methacrylamide dopamine hydrogels containing Ti_3C_2 MXene can also reduce inflammation and facilitate water/air transport whit long-term antibacterial effects, remarkably on *S. epidermidis*, which has been rarely studied in MXene skin wound repair devices. Possessing high ROS scavenging capacities (96% scavenging ratio at 120 minutes) the wound closure rate increased from 39% to 81% within 7 days with increased neoangiogenesis due to VEGF and TGF-β1 expression.[103]

Even if not specifically mentioned in this paragraph, other MXene-based solutions have been tested against multidrug-resistant species, though not precisely for wound healing applications.[104–106]

5.3. Wound healing for cancer treatment

With the increasing incidence of cutaneous melanoma, there is a growing focus on understanding the best surgical treatment strategies. The primary recommended standard of care is wide local excision surgery, where the tumor is removed with a margin of clinically unaffected skin. However, less than 1% of the surgical margin is examined, leading to significant recurrence rates. As a result, alternative surgical methods, such as Mohs micrographic surgery (MMS), have been proposed since it conserves tissue while examining nearly 100% of the margin. MMS is particularly suitable for skin tumors with a high likelihood of recurrence and for cancers located in areas where preserving skin is critical. When a lesion is relatively large, especially on the face, it is more likely that a flap or graft would be necessary, making MMS the preferred excision method.[110,111] To kill remaining cells and/or boost the immune system, radiotherapy (RT) can be used to induce DNA damage in cancer cells. Adjuvant RT to the primary lesion is typically recommended for patients at high risk of recurrence, particularly those with desmoplastic neurotropic melanoma and lesions in the head and neck region. Other indications for adjuvant RT include tumors thicker than 4 mm, the presence of ulceration, satellitosis, positive surgical margins, and mucosal origin.[112] RT is also considered a viable alternative to surgery for medically inoperable patients, those who refuse surgery, or when surgery might result in poor cosmetic outcomes.[113] Imiquimod-based treatment therapy can also be exploited for local treatments since it can penetrate the epidermal barrier, and act as an agonist for Toll-like receptors, which initiate the innate immune response and bridge to adaptive immunity. Additionally, imiquimod can be used as a neoadjuvant, adjuvant, or complementary therapy.[114]

As described in section 1, MXene-based PTT impairs both bacteria and cancer cells. Besides systemic MXene-based melanoma drug delivery systems based on photothermal effects[115] or delivery of molecules such as pH-sensitive quercetin $Ti_3C_2T_x$ nanoparticles,[116] local melanoma treatment with MXene-based patches has been proposed by a few groups, as summarized in Table 3. Dong and colleagues created a $Ti_3C_2T_x$ doxorubicin-loaded agarose hydrogel for infrared-mediated release of chemotherapeutic that efficiently killed mouse melanoma cells *in vitro* after 5 minutes at 808 nm,.[107] TNF-α can be also released from MXene-agarose gels to obtain NIR light-controllable pro-apoptotic signalling in cancer spheroids (HCT116 cells).[91]

Since many devices possess unequal thermal distribution between the upper part and the lower part that contacts skin, Ding and colleagues designed a $Ti_3C_2T_x$ gelatine PLA membrane with advanced thermal management during NIR irradiation.[108] The MXene coating on the upper surface generated heat, which was efficiently transferred to the lower surface due to the superior thermal properties of MXene and its ability to enhance infrared thermal radiation. The improvement of the unidirectional thermal conductivity allowed for NIR-mediated antibacterial effects even against antibiotic-resistant species, cancer treatment, and wound healing at the same time.

An electrostimulation-augmented photothermal patch (eT-patch) comprising poly (acrylamide-*co*-acrylic acid) $Ti_3C_2T_x$ hydrogel has been developed by Ju and colleagues (Fig. 11 from ref. 117). eT-patch is transparent and biocompatible with healthy tissues and can trigger apoptosis and pyroptosis in melanoma cancer cells both *in vitro* and *in vivo.*[109] Similarly, Zheng *et al.* designed a multi-responsive electronic skin (e-skin) for on-demand drug delivery, designed to facilitate melanoma postoperative therapy. The e-skin has been constructed using a natural porcine dermal matrix, MXene nanosheets, silver nanowires, and mesoporous hollow silica microspheres for doxorubicin drug-loading. e-skin exhibits responsiveness to temperature, pH, and electric stimulation,

Table 3 Cancer Wound dressing using MXenes

Composition	Antibacterial mechanism/tested species	Tissue regeneration/therapeutic effects/other	Triggering mechanism/sensor	Ref.
$Ti_3C_2T_x$ doxorubicin agarose hydrogel	—	Mouse melanoma cells (B16-F10) killing mediated by Dox	Infrared mediated thermal increase and release of drugs from the hydrogel	107
Ti_3C_2 agarose/HgF, Agarose/TNF-α	—	Wound healing, anticancer effects (subcutaneous HCT116 tumours in mice)	NIR-mediated release of drugs	91
$Ti_3C_2T_x$ PLA gelatin electrospun nanofibers	*E. coli* and *S. aureus MRSA*	Cancer treatment (subcutaneous B16F10 tumours in mice), wound healing (rats) and antibacterial effects	Photostimulation	108
$Ti_3C_2T_x$ Poly (acrylamide-*co*-acrylic acid) hydrogel, eT-patch	—	Melanoma treatment *via* photothermal and ES in melanoma-bearing C57BL/6J mice model	Photostimulation ES	109
Porcine acellular dermal matrix (PADM), MXene, silver nanowires (AgNWs), doxorubicin microspheres ($TSOHSiO_2$ @Dox), PADM-MX-Ag-Si@Doxe-skin	AgNWs and MXene efficacy against, *S. aureus* and *E. coli*	Melanoma post-operative therapy (anticancer effects of Dox) and wound-healing acceleration in C57BL/6 mice	Doxorubicin release Triggered by body temperature, pH, ES	84

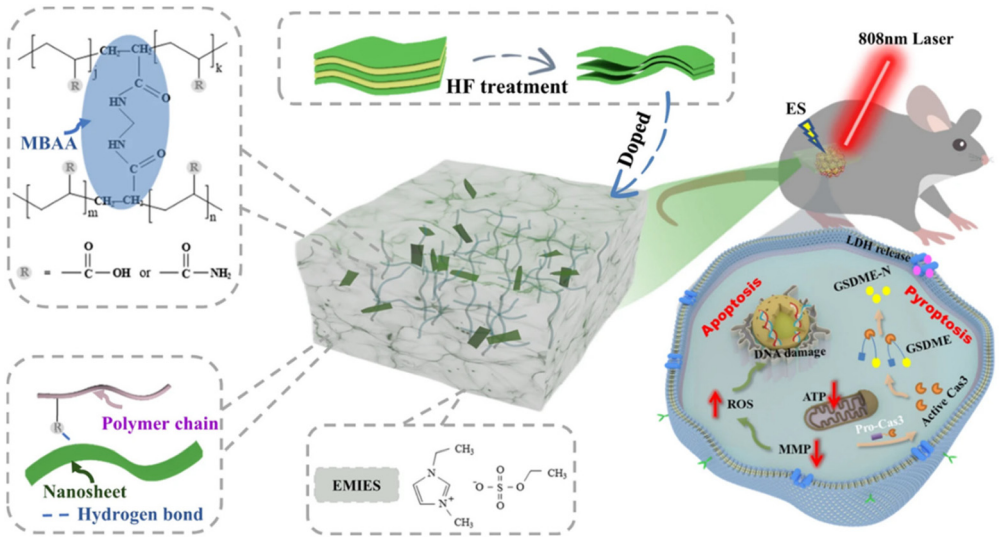

Fig. 11 eT-patch used for PTT treatment combined with ES. The patch is made up of ionic gel doped with MXene's nanosheets ($Ti_3C_2T_x$). Reproduced with permission from ref. 117 under Creative Common license.

enabling controlled drug release with strong antibacterial effects against *S. aureus* and *E. coli* and support of electrophysiological activities that enhance wound healing and therapeutic control while monitoring pH changes, cell proliferation, and tumor size (Fig. 12 from ref. 84).

6. Combined wound healing and sensing

Wearable sensors based on MXenes are numerous and have been discussed in other excellent Reviews.[118–122] In this section, we will focus on sensor systems such as hydrogels, microneedles patches, or fabric that also have specific activities for skin wound healing, summarized in Table 4.

As discussed in the previous section, in cancer wound healing devices such as et-Patch or e-skin, the antibacterial or regenerative effects can be combined with wearable sensors, with MXenes offering improved conductivity and controllable responsiveness to NIR for drug release, or capability of local ES.[84,109,123]

$Ti_3C_2T_x$ nanosheets deposited on cellulose nonwoven fabric exhibit sensitive and reversible humidity response enabling wearable respiration monitoring. They can also serve as low-voltage thermotherapy to kill *S. aureus* in rat skin wounds and enhance wound healing when electrically stimulated.[124]

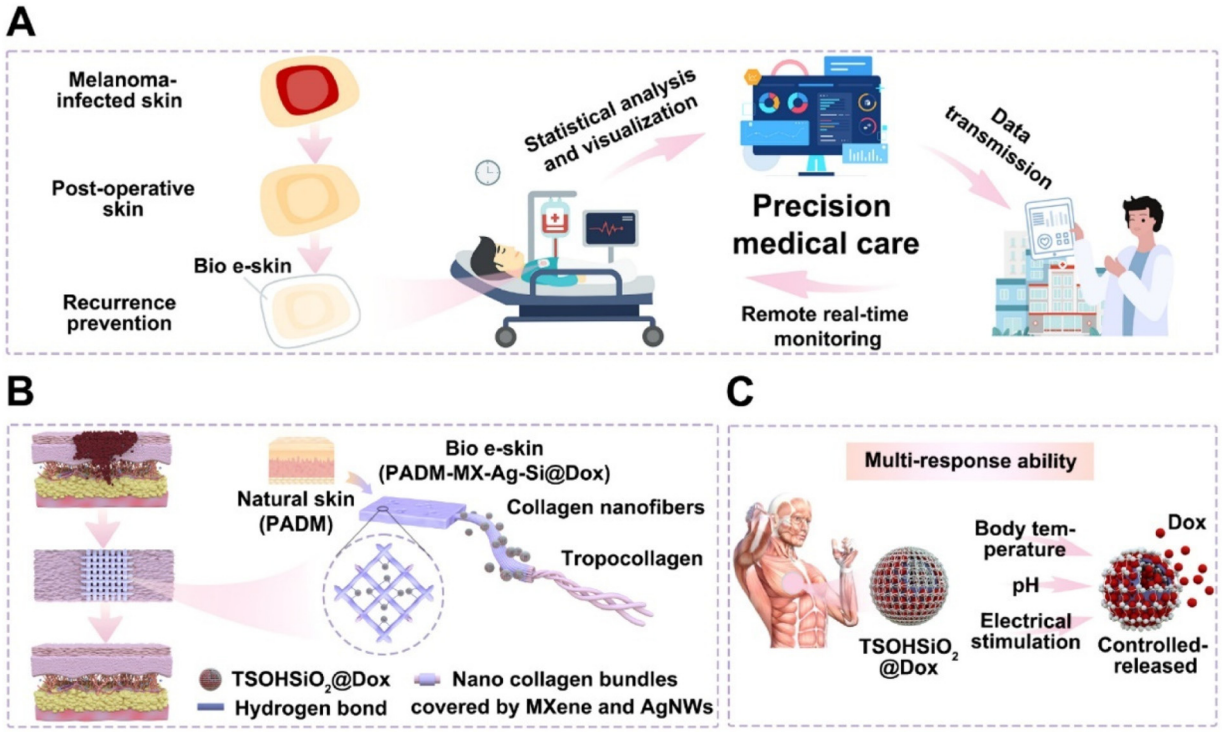

Fig. 12 (A) Schematic illustration of Bio e-skin used in precision medical care. (B) Components of Bio e-skin (PADM-MX-Ag Si@Dox) include nano-collagen bundles coated by MXene and AgNWs and linked to $TSOHSiO_2$@Dox particles. (C) Multi-response ability to pH, temperature and electrical stimulation is given by nanoparticles to regulate Dox release. Adapted with permission from ref. 84. Copyright 2024 Published by Elsevier Ltd on behalf of the editorial office of Journal of Materials Science & Technology.

In the AgNPs/$Ti_3C_2T_x$ guar gum and phenylboronic acid grafted sodium alginate hydrogel for cardiovascular and muscle-related diseases diagnosis and wound repair, besides the improved mechanical strength and conductivity, an effective rheological self-healing property, with ductility and stretchability has been achieved (Fig. 13 from ref. 133). This hydrogel degraded within 45 days in PBS and had no evident cytotoxicity. The hydrogel had antibacterial effects due to the embedded silver nanoparticles with *in vivo* wound repair demonstrated after 12 days. When a wearable epidemic sensor was produced with the hydrogel, it recorded wrist bending motions, pulse performance, and electrophysiological signals (such as ECG and EMG signals) with a higher signal-to-noise ratio than commercial electrodes.[85] $Ti_3C_2T_x$-based sensor with silver-mediated antibacterial effects can respond to electrical stimuli that enhance wound healing even in diabetic rats, while providing electromechanical responsiveness. The hydrogels maintained stability and functionality over 100 cycles of pressure and strain, indicating excellent mechanical and electrochemical reliability. The incorporation of MXene nanosheets and zwitterions in the hydrogel forms conductive pathways, enhancing the resistance changes under stress, which contributed to their high sensitivity.[87]

Recording patient movement can be beneficial for wound healing monitoring and prompt intervention. A microneedle $Ti_3C_2T_x$-based patch with a geometry inspired by Shark Tooth or intestinal wrinkles was reported by Gao and colleagues using a two-step method that envisaged MXene solution pouring on a pre-stretched silicone rubber mold modified with laser patterned conical grooves (Fig. 14 from ref. 134). Silk fibroin, polyurethane, and silk protein spidroin were then poured as a supporting substrate. This elastic film was sensitive to motion when attached to human skin thanks to MXene electrical conductivity and demonstrated *in vivo* wound healing effects mediated by NIR-controlled release of human epidermal growth factor (hEGF).[125–127] The same technique for microneedle synthesis was used to obtain a patch capable of pH, glucose, and motion monitoring.[125–127] $Ti_3C_2T_x$, silk spydroin and aloe vera gel have been 3D-printed or used as temperature microneedle NIPAM sensors to repair and/or monitor wound healing in mice.[128]

MXenes have been also combined with graphene to obtain a multifunctional hydrogel scaffold made of chitosan/human-like collagen composites along with the 2D materials. The hydrogel induced hemostasis, moisture permeability, mechanical flexibility, electroactivity, and self-healing capabilities and promote healing through the delivery of electrical signals to the wound.[129]

Due to their self-powered capabilities, Triboelectric nanogenerators (TENGs), which are miniature self-powered devices that can harvest mechanical energy from body movements such as breathing, heartbeat, and limb motions, and convert it into electrical energy have garnered significant interest in

Table 4 Wound healing sensors based on MXenes

Composition	Proven antibacterial effects	Therapeutic effects/other	Sensing properties	Ref
$Ti_3C_2T_x$ poly (acrylamide-*co*-acrylic acid) hydrogel eT-patch	—	Melanoma treatment *via* photothermal and ES in melanoma-bearing C57BL/6J mice model	Can conduct current (5 V) and light up a commercial light-emitting diode according to MXene concentration used	109
Porcine acellular dermal matrix (PADM) MXene, silver nanowires (AgNWs), doxorubicin microspheres ($TSOHSiO_2$ @Dox), PADM-MX-Ag-Si@Dox, e-skin	AgNWs and MXene efficacy against *S. aureus* and *E. coli*	Melanoma post-operative therapy (anticancer effects of Doxorubicin) and wound-healing acceleration in C57BL/6 mice (ES)	Sensor for body temperature, pH, humidity, motion sensor	84
$Ti_3C_2T_x$ PNIPAm polymer. γ-Methacryloxypropyltrimethoxysilane (KH570)	—	Biocompatible with induction of thicker epidermidis and follicles *in vivo*. NIR controllable properties (Tetracycline release)	Broad range strain sensitivity, fast response, and good cycle stability. Motion and bending sensor	123
$Ti_3C_2T_x$ nanosheets deposited on cellulose nonwoven fabric	Photothermal killing *S.aureus*	Electrically stimulated PTT and wound healing in SD rats	Humidity and motion sensor	124
AgNPs/$Ti_3C_2T_x$ guar gum (GG) phenylboronic acid grafted sodium alginate (Alg-PBA) injectable sensor	AgNPs efficacy against *S. aureus* and *E. coli*	Wound healing	Can be used as epidermic sensor for wrist bending motions, wrist pulse performance, electrophysiological signals	85
silk-fibroin AgNP nanoparticle PDA $Ti_3C_2T_x$ acrylamide	AgNPs efficacy against *S. aureus* and *E. coli*	Wound healing in SD rats with diabetes, antibacterial effects due to silver nanoparticles, neoangiogenesis due to ES	Electromechanical sensor, senses pressure and motion for multiple cycles	87
Microneedle dressing Polyurethane, spidroin $Ti_3C_2T_x$	—	hEGF mediated wound healing	Motion sensor	125–127
$Ti_3C_2T_x$ silk spydroin NIPAM	—	Photothermal release and wound healing in mice	Motion sensor	128
Graphene MXene hyperbranched Polyglycidyl ether polymer-based multifunctional hydrogel scaffold made of chitosan/human-like collagen composites	*S. aureus*, *E. Coli*	Wound healing in mice due to ES	Motion sensor	129
Gelatin/Ecoflex/Ti_3C_2	—	Wound healing in mice (NIR-mediated or ES)	TENG sensor for coughing, swallowing and speaking, motion sensor	130
PVA/Ecoflex/$Ti_3C_2T_x$ /borate/gly(glycerol) hydrogel and Ecoflex	—	Diabetic rat full-thickness wound model (ES) promoting cell proliferation and migration, collagen deposition and angiogenesis	TENG sensor monitors human movement	93
$Ti_3C_2T_x$ PDA silver poly(acrylamide-*co*-sulfobetaine methacrylate) hydrogel	*S. aureus*, *E. coli*	Skin wound model on type I diabetic rats Silver ions (antibacterial effects), ES for wound healing	Bending sensor, heartbeat sensor	131
Phenylboronic acid-modified flaxseed gum and PVA-PDA-grafted MXene, chlorogenic acid, L-ascorbate-2-phosphate trisodium salt, and exosomes derived from adipose-derived stem cells	*E. coli*, *S. aureus*, and *P. aeruginosa*	Mice model of type I diabetes wounds, chlorogenic acid antibacterial effects	ROS/glucose-stimulated release of exosomes	132

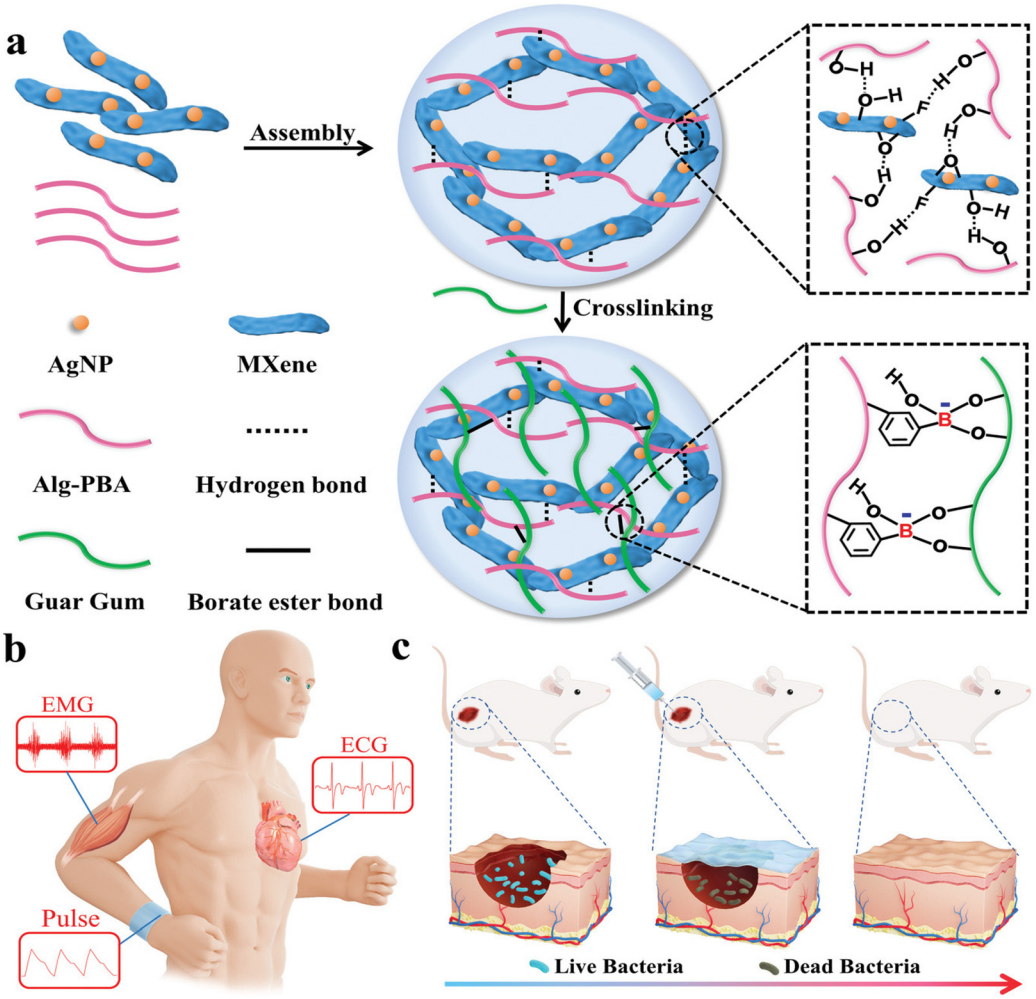

Fig. 13 Illustration of multifunctional MXene hydrogel wound healing sensor assembly. The different constituents are reported in (a): AgNP, Alg-PBA, Guar Gum and MXene interact *via* hydrogen bonds and borate ester bonds to produce the desired hydrogel. (b) and (c) Represent potential applications to medical monitoring and skin infections, respectively. Reproduced with permission from ref. 133. Copyright 2022 Wiley-VCH GmbH.

wearables devices. The TENG Ti_3C_2 skin sensor made with gelatin and Ecoflex has both NIR and electroactive properties that have been combined *in vivo* for mice wound healing.[130] In the electrically stimulated mice group, the wound area is reduced significantly – in association with new blood vessel formation and both the collagen fiber content and hair follicle density are increased. The use of another TENG band-aid made with PVA/Ecoflex/$Ti_3C_2T_x$/borate/gly(glycerol) hydrogel repaired diabetic rat full-thickness wounds.[93] Furthermore, it was found that the hydrogel's mechanical strength increased compared to the control, and cell proliferation rate was enhanced by ES. *In vivo* experiments on diabetic rats showed that wounds treated with the Band-Aid healed faster compared to the control group. $Ti_3C_2T_x$ PDA silver poly(acrylamide-*co*-sulfobetaine methacrylate) stretchable and biocompatible hydrogel has also been designed to achieve both sensing and wound healing in diabetic rats. The hydrogel has been enriched with silver ions to kill *S. aureus* and *E. coli.*[131] The sensing capabilities have been tested for finger and elbow bending, knee bending while walking, jogging, and running, and long-term heartbeat monitoring in rats.

As depicted in section 4.2, diabetic wounds remain in a hyperglycaemic environment for extended periods, leading to prolonged oxidative stress at the wound site and significantly higher levels of H_2O_2 and glucose in the microenvironment. Consequently, a hydrogel that responds to ROS and glucose has been designed using a phenylboronic acid-modified flaxseed gum and PVA to form a dynamic phenylboronate ester.[132] This hydrogel has been enriched with a blend of PDA-grafted MXene, chlorogenic acid, L-ascorbate-2-phosphate trisodium salt, and exosomes derived from adipose-derived stem cells. The catechol structure in PDA imparts strong wet tissue adhesion, while chlorogenic acid provides antioxidant and antibacterial properties. This combination, along with stimuli-responsive exosome release, accelerates healing, promotes wound angiogenesis, and reduces ROS and inflammatory responses. It has been shown that this ROS/glucose-responsive hydrogel system can reduce ROS and inflammatory responses

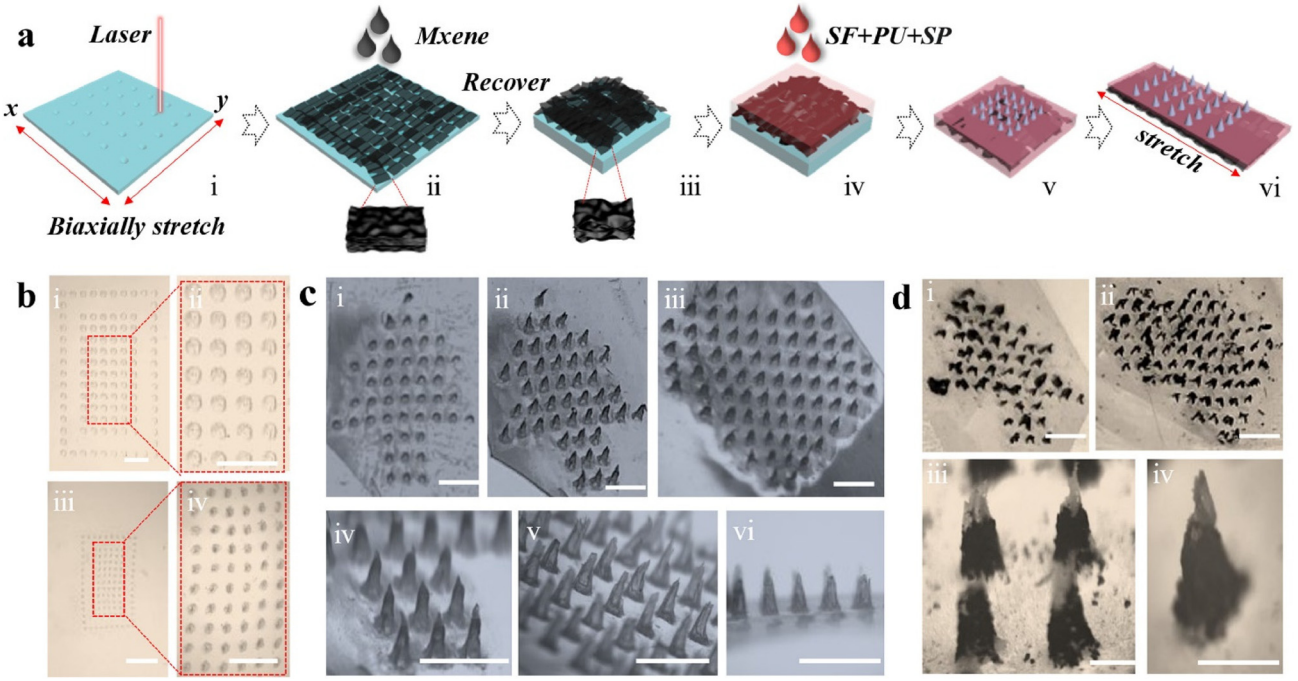

Fig. 14 (a) Schematic figure of the steps followed for the fabrication of Mxene-based microneedle dressing, consisting of silk fibroin (SF), polyurethane (PU), and spidroin (SP). (b) Illustrates the pattern of Ecoflex mold. (c) Shows the morphology of dressings observed by microscopy. (d) Micrographs of different patterns. Reproduced with permission from ref. 134. Copyright 2023 Acta Materialia Inc. Published by Elsevier Ltd. All rights reserved.

by repairing the electron transfer chain, thereby promoting skin damage repair in a mouse model of type I diabetes as shown in Fig. 15 from ref. 132.

7. Future perspectives

We have described many examples of treatment based on MXenes, from chronic wounds to diabetic, and cancer wounds. Some applications for other skin conditions exist and might be treated with MXenes in the future. For example, psoriasis topical treatment can help to protect the affected skin from further irritation and scratching, which can inhibit infection and promote healing. Additionally, the development of new wound dressing technologies might help to maintain moisture in the skin, reducing dryness and flakiness. However, there is a lack of MXenes-based antibacterial bandages specifically designed for psoriasis. Psoriasis therapies include chemical agents, corticosteroids, and stem cell transplantation but, so far, only IL-17 monoclonal antibodies (mAbs) have been used specifically for psoriatic treatment in combination with MXenes.[83]

Also, atopic dermatitis, a skin condition dependent on Th2-cells, cytokine, immunoglobulin E, and eosinophilic responses might benefit from MXene regulation of immune response.[135–138] As an example of immune regulation by MXene nanoparticles, vanadium carbide (V_2C) MXenes represent enzyme-mimic nanomaterials with adjustable ROS-scavenging catalytic activity. When combined with DNase-I they can disassemble biofilms and reorientate neutrophil functions. Indeed, V_2C ROS scavenging reduces the release Of NETs from neutrophils by inhibiting the ROS–neutrophil elastase/myeloperoxidase–peptidylarginine deiminase 4 pathway and enhances the phagocytic activity of neutrophils through activating the ROS–PI3K–AKT–mTOR pathway, thereby skewing neutrophils from NETosis toward phagocytosis. Besides, with the remodelling of the microenvironment, DNase-I activity is maintained for long-term, augmenting its penetration depth in biofilms, thereby completely degrading eDNA and NETs. Biofilm lysis further facilitates the functional conversion of neutrophils and accelerates the elimination of bacteria and biofilm debris through phagocytosis in diabetic wounds (Fig. 16 from ref. 139).

Melanoma treatment has been proposed with doxorubicin, but other drugs might be combined with MXenes patches to create new regenerative therapies. Indeed Electrochemotherapy (ECT) is one of the applications of electroporation (EP) and is currently employed in clinical practice to treat cutaneous and subcutaneous tumors, particularly melanoma. The combination of EP with chemotherapy significantly reduces the need for surgical intervention, allows for localized cancer treatment, lowers the required drug dose, and minimizes the side effects of systemic chemotherapy.[140] ECT enhances drug delivery by using EP to destabilize the cell membrane, facilitating drug

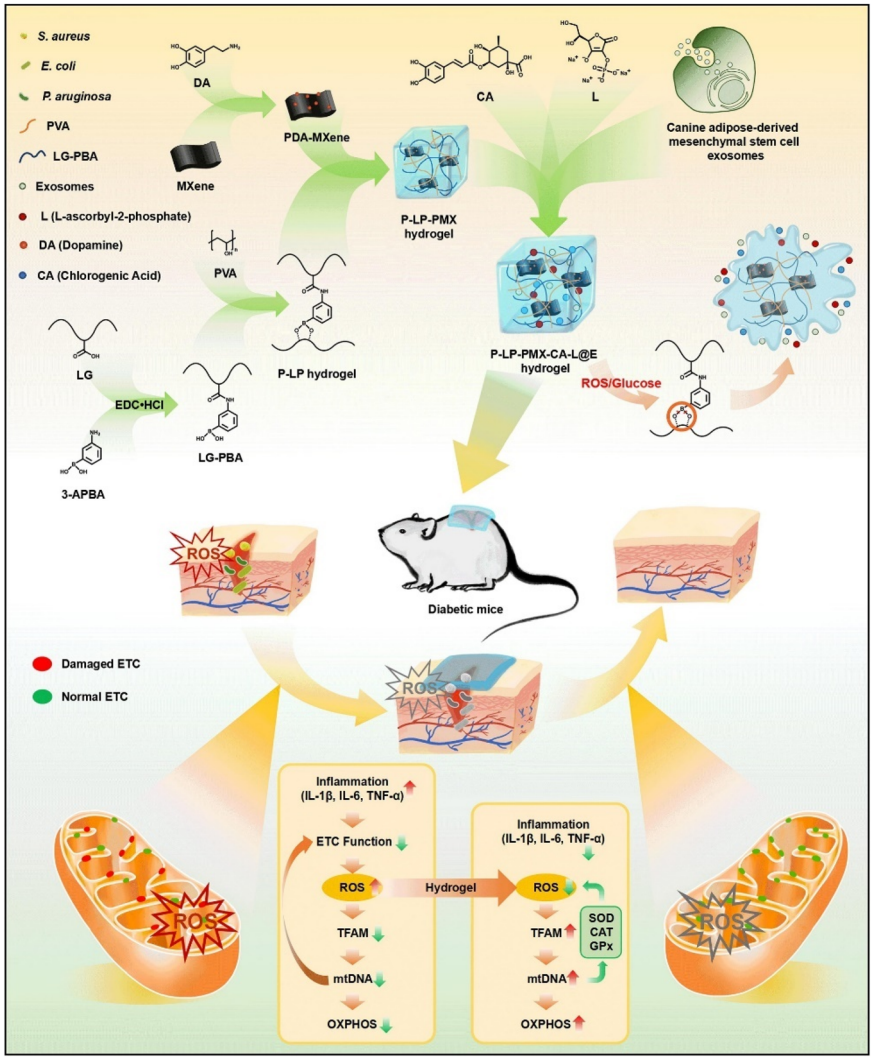

Fig. 15 Schematic illustration of experimental setup and biochemical mechanisms of hydrogel that responds to ROS and glucose designed using a phenylboronic acid-modified flaxseed gum and PVA to form dynamic phenylboronate ester. This hydrogel has been enriched with a blend of PDA-grafted MXene, chlorogenic acid, L-ascorbate-2-phosphate trisodium salt, and exosomes derived from adipose-derived stem cells. Reproduced with permission from ref. 132. Copyright 2024 Elsevier B.V. All rights reserved.

diffusion into the cells and thereby enhancing the local cytotoxic effect. Two cost-effective agents commonly used in ECT are bleomycin and cisplatin, both of which have demonstrated significant tumor size reduction in malignant melanoma.[141,142] In melanoma patients receiving anti-PD1 immunotherapy with pembrolizumab, ECT has been shown to enhance local response and tumor control on cutaneous metastases without significant toxicity. The application of electric pulses also generates ROS, which plays a role in the cell death signalling cascades, further stimulating the innate immune system.[142] ECT and bleomycin-cisplatin combination might be a future therapy to test exploiting NIR-mediated release from MXene hydrogels together with their electrical conductivity. Injectable MXene hydrogels might also be exploited with unresectable, recurrent, or refractory melanoma with cutaneous, subcutaneous, or nodal metastases. Include intralesional injection of oncolytic viruses, such as Talimogene laherparepvec (T-VEC), the first genetically modified herpes simplex virus-1-based oncolytic Food and Drug Administration (FDA) approved immunotherapy. This intratumorally injectable drug is engineered to preferentially replicate within tumors and stimulate antitumor immune responses both locally and systemically.[143] Finally, the treatment of non-melanoma skin cancer has not been studied, as an example MXenes might be exploited in combination with drugs such as retinoids.[144]

Bacterial infections of the skin are commonly caused by various species, with *Staphylococcus aureus* and Streptococcus pyogenes being the most prevalent. *S. aureus*, including MRSA, is notorious for causing abscesses and wound infections, while Streptococcus pyogenes is frequently associated with conditions such as erysipelas and

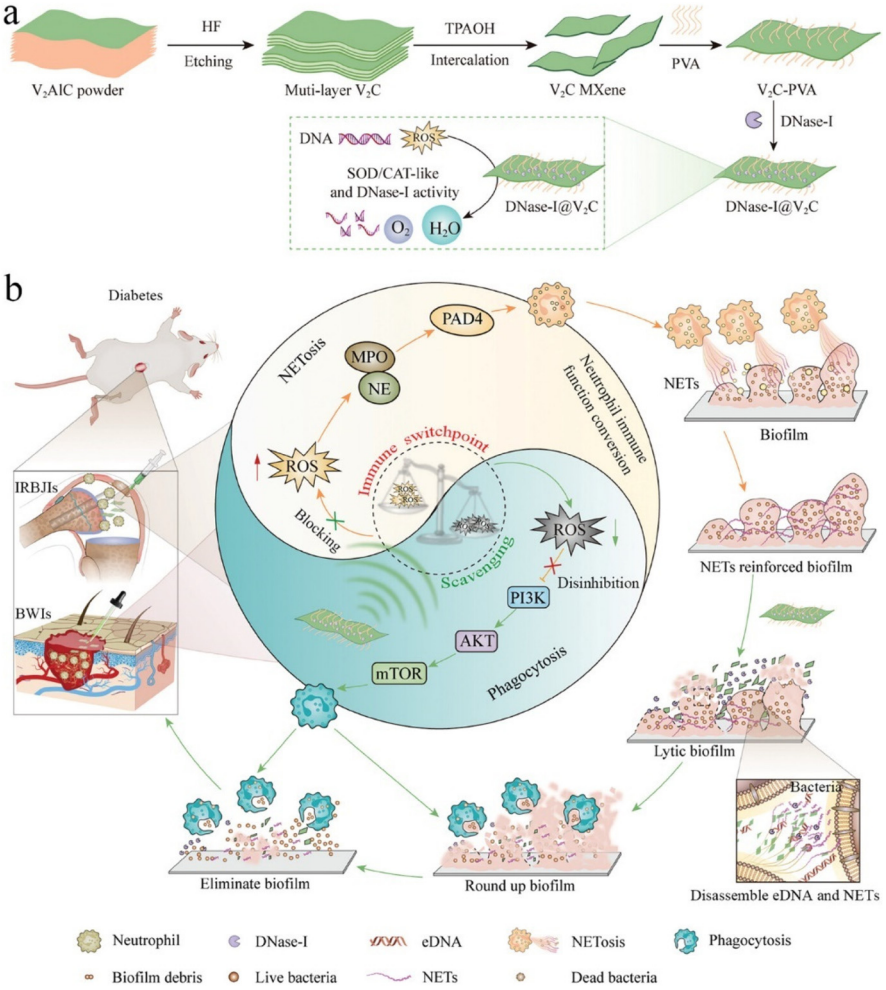

Fig. 16 Illustration of (a) synthesis of DNAse-I@V2C MXenes and (b) their role in fighting biofilm infections linked to diabetic pathology. Reproduced with permission from ref. 139. Copyright 2023 Wiley-VCH GmbH.

scarlet fever. Though many patches have been tested against *S. aureus* and *E. coli*, other bacterial species have been poorly tested, future MXenes research might focus on S. pyogenes as well as fungal species responsible for dermatological infection.[145]

It is also important to consider that all tests conducted so far have been performed *in vivo* on mice or rats. However, the principle of the 3Rs advocates for the replacement of animal testing with more sustainable *in vitro* models,[146] including 3D bioprinting and lab-on-a-chip testing technologies. Incorporating these advanced *in vitro* models in the field of 2D materials can enhance the precision and ethical standards of research, potentially accelerating the development of effective treatments while reducing reliance on animal models (see section 2).

Although there have been advancements in wound monitoring, the development of techniques based on artificial intelligence (AI) of the dressing itself is still lacking.[147] In 2022, Kalasin and colleagues focused on the development of a binary wearable system that integrates an AI-guided sensor with a smart, battery-free bandage for chronic wound monitoring.[148] The $Ti_3C_2T_x$ MXene-based system tracked the skin healing stages of participants with pruritic conditions treated with topical corticosteroids. The healing process was classified into three phases: inflammation, proliferation, and remodelling, using pH-responsive voltage as a key indicator. Real-time data from the wearable sensor were processed through a deep artificial neural network algorithm and the wearable sensor displays the healing progress on an integrated LCD screen. The system demonstrated a 94.6% accuracy in recognizing healing stages and provided efficient real-time monitoring of treatment efficacy in patients with various skin conditions, *i.e.*, allergic skin rash, urticaria, psoriasis, and chronic dermatitis (Fig. 17 from ref. 148).

In the near future, the AI-based wound dressing might itself possess antibacterial or electrical stimulating properties for wound healing. Also, new research may directly print MXenes wound dressing on patients using *in situ* bioprinting with robotic arm following the 3D tissue morphology by a scanning software.[149,150]

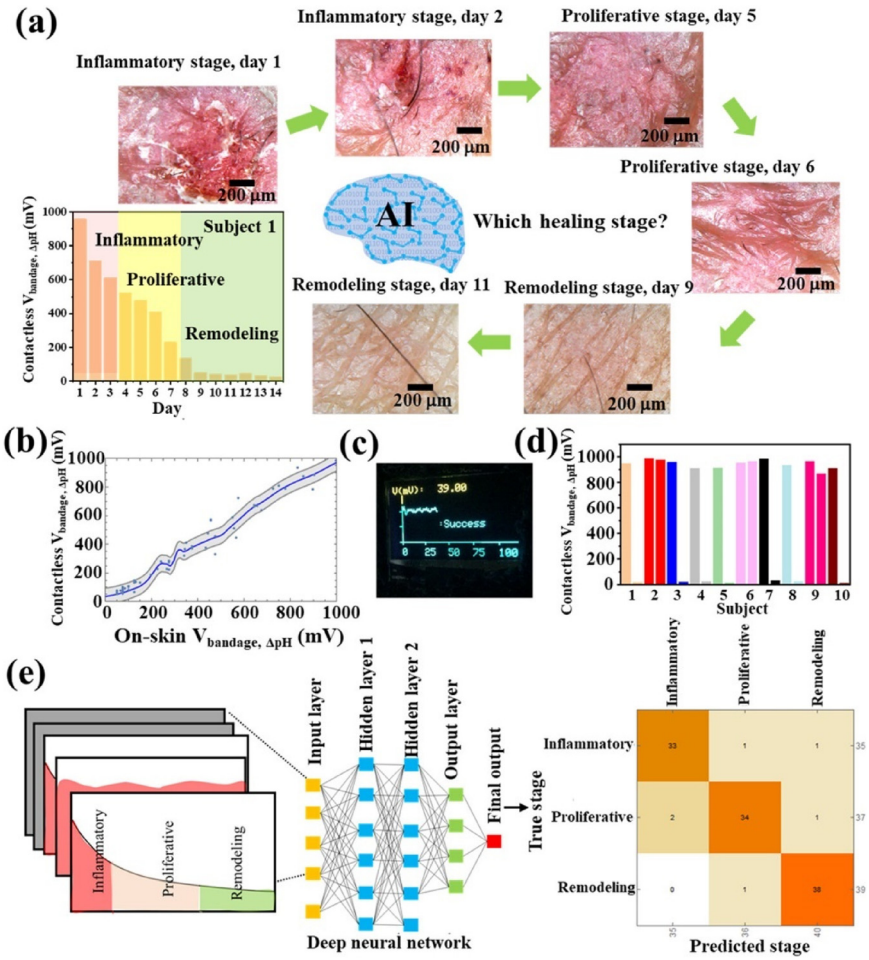

Fig. 17 (a) Shows the healing process measurements collected from a person with inflamed skin. (b) Illustrates pH-responsive voltages. (c) Represents a wearable device designed for skin. (d) Data was collected from the device during a time up to 14 days. (e) Example of classification of inflammatory, proliferative and remodeling stages. Reproduced with permission from ref. 148. Copyright 2022 American Chemical Society.

8. Conclusions

This review emphasizes the potential of MXenes in revolutionizing skin wound healing through their unique multifunctional properties. The development of MXenes-based hydrogels and patches has demonstrated significant advancements in antibacterial efficacy, tissue regeneration, and real-time monitoring capabilities. These materials not only enhance the healing process but also provide a robust framework for integrating sensors that monitor critical wound parameters. Future research should focus on optimizing the synthesis and functionalization of MXenes to further improve their biocompatibility and therapeutic efficacy. The promising results from *in vivo* experiments highlight the need for clinical trials to validate the safety and effectiveness of MXenes-based treatments. Ultimately, the incorporation of MXenes into advanced wound care solutions holds great promise for addressing the challenges of chronic and non-healing wounds, offering a new horizon in biomedical applications.

Data availability

No primary research results, software or code have been included and no new data were generated or analysed as part of this review.

Conflicts of interest

There are no conflicts to declare.

Acknowledgements

This work was supported by PRIN-PNRR Project WOUNDXENE, Project n°202274SLX8, CUP B53D23008580006, funding scheme "PIANO NAZIONALE DI RIPRESA E RESILIENZA (PNRR) – Missione 4 "*Istruzione e Ricerca*" – Componente C2; Investimento 1.1, "*Fondo per il Programma Nazionale di Ricerca e Progetti di Rilevante Interesse Nazionale*

(PRIN)"; Decreto Direttoriale n. 104 del 2 febbraio 2022, financed by European Union – NextGenerationEU. V. P. acknowledges Project PNC 0000001 D3 4 Health, CUP B53C22006100001, The National Plan for Complementary Investments to the NRRP, Funded by the European Union – NextGenerationEU".

References

1 P. Kolimi, S. Narala, D. Nyavanandi, A. A. A. Youssef and N. Dudhipala, Innovative treatment strategies to accelerate wound healing: trajectory and recent advancements, *Cells*, 2022, **11**, 2439.

2 F. Seidi, A. Arabi Shamsabadi, M. Dadashi Firouzjaei, M. Elliott, M. R. Saeb, Y. Huang, *et al.*, MXenes antibacterial properties and applications: a review and perspective, *Small*, 2023, **19**, 2206716.

3 S. Iravani and R. S. Varma, MXenes and MXene-based materials for tissue engineering and regenerative medicine: Recent advances, *Mater. Adv.*, 2021, **2**, 2906–2917.

4 Y. Hu, F. Wang, H. Ye, J. Jiang, S. Li, B. Dai, *et al.*, MXene-based flexible electronic materials for wound infection detection and treatment, *npj Flexible Electron.*, 2024, **8**, 30.

5 J. A. Kumar, P. Prakash, T. Krithiga, D. J. Amarnath, J. Premkumar, N. Rajamohan, *et al.*, Methods of synthesis, characteristics, and environmental applications of MXene: A comprehensive review, *Chemosphere*, 2022, **286**, 131607.

6 M. Naguib, V. N. Mochalin, M. W. Barsoum and Y. Gogotsi, 25th anniversary article: MXenes: a new family of two–dimensional materials, *Adv. Mater.*, 2014, **26**, 992–1005.

7 M. Naguib, M. Kurtoglu, V. Presser, J. Lu, J. Niu, M. Heon, *et al.*, Two-dimensional nanocrystals produced by exfoliation of Ti_3AlC_2, *MXenes*, 2011, 15–29.

8 B. Anasori, Y. Xie, M. Beidaghi, J. Lu, B. C. Hosler, L. Hultman, *et al.*, Two-dimensional, ordered, double transition metals carbides (MXenes), *ACS Nano*, 2015, **9**, 9507–9516.

9 L. Gao, C. Li, W. Huang, S. Mei, H. Lin, Q. Ou, *et al.*, MXene/polymer membranes: synthesis, properties, and emerging applications, *Chem. Mater.*, 2020, **32**, 1703–1747.

10 Y. Gogotsi and B. Anasori, The rise of MXenes, *ACS Nano*, 2019, 8491–8494.

11 M. Naguib, M. W. Barsoum and Y. Gogotsi, Ten years of progress in the synthesis and development of MXenes, *Adv. Mater.*, 2021, **33**, 2103393.

12 A. Feng, Y. Yu, Y. Wang, F. Jiang, Y. Yu, L. Mi, *et al.*, Two-dimensional MXene Ti_3C_2 produced by exfoliation of Ti_3AlC_2, *Mater. Des.*, 2017, **114**, 161–166.

13 R. Meshkian, L.-Å. Näslund, J. Halim, J. Lu, M. W. Barsoum and J. Rosen, Synthesis of two-dimensional molybdenum carbide, Mo_2C, from the gallium based atomic laminate Mo_2Ga_2C, *Scr. Mater.*, 2015, **108**, 147–150.

14 Y. Gogotsi, Transition metal carbides go 2D, *Nat. Mater.*, 2015, **14**, 1079–1080.

15 A. Rosenkranz, G. Perini, J. Y. Aguilar-Hurtado, D. F. Zambrano, B. Wang, B. Niccolini, *et al.*, Laser-Mediated Antibacterial Effects of Few-and Multi-Layer $Ti_3C_2T_x$, *MXenes*, 2021, 150795.

16 M. Khazaei, A. Ranjbar, M. Arai, T. Sasaki and S. Yunoki, Electronic properties and applications of MXenes: a theoretical review, *J. Mater. Chem. C*, 2017, **5**, 2488–2503.

17 F. Shahzad, A. Iqbal, H. Kim and C. M. Koo, 2D transition metal carbides (MXenes): applications as an electrically conducting material, *Adv. Mater.*, 2020, **32**, 2002159.

18 M. Overchuk, R. A. Weersink, B. C. Wilson and G. Zheng, Photodynamic and photothermal therapies: synergy opportunities for nanomedicine, *ACS Nano*, 2023, **17**, 7979–8003.

19 D. Xu, Z. Li, L. Li and J. Wang, Insights into the photothermal conversion of 2D MXene nanomaterials: synthesis, mechanism, and applications, *Adv. Funct. Mater.*, 2020, **30**, 2000712.

20 D. Zhang, D. Shah, A. Boltasseva and Y. Gogotsi, MXenes for photonics, *ACS Photonics*, 2022, **9**, 1108–1116.

21 P. Zijlstra, P. M. R. Paulo and M. Orrit, Optical detection of single non-absorbing molecules using the surface plasmon resonance of a gold nanorod, *Nat. Nanotechnol.*, 2012, **7**, 379–382.

22 X. Fan, L. Liu, X. Jin, W. Wang, S. Zhang and B. Tang, MXene Ti 3 C 2 T x for phase change composite with superior photothermal storage capability, *J. Mater. Chem. A*, 2019, **7**, 14319–14327.

23 S. Kyrylenko, O. Gogotsi, I. Baginskiy, V. Balitskyi, V. Zahorodna, Y. Husak, *et al.*, Mxene-assisted ablation of cells with a pulsed near-infrared laser, *ACS Appl. Mater. Interfaces*, 2022, **14**, 28683–28696.

24 T. R. Dmytriv and V. I. Lushchak, Potential Biosafety of Mxenes: Stability, Biodegradability, Toxicity and Biocompatibility, *Chem. Rec.*, 2024, e202300338.

25 V. Palmieri, F. Bugli, M. C. Lauriola, M. Cacaci, R. Torelli, G. Ciasca, *et al.*, Bacteria Meet Graphene: Modulation of Graphene Oxide Nanosheet Interaction with Human Pathogens for Effective Antimicrobial Therapy, *ACS Biomater. Sci. Eng.*, 2017, **3**, 619–627.

26 J.-H. Jang and E.-J. Lee, Influence of MXene particles with a stacked-lamellar structure on osteogenic differentiation of human mesenchymal stem cells, *Materials*, 2021, **14**, 4453.

27 K. Rasool, M. Helal, A. Ali, C. E. Ren, Y. Gogotsi and K. A. Mahmoud, Antibacterial activity of $Ti_3C_2T_x$ MXene, *ACS Nano*, 2016, **10**, 3674–3684.

28 T. R. Dmytriv and V. I. Lushchak, Potential Biosafety of Mxenes: Stability, Biodegradability, Toxicity and Biocompatibility, *Chem. Rec.*, 2024, e202300338.

29 G. Perini, A. Rosenkranz, G. Friggeri, D. Zambrano, E. Rosa, A. Augello, *et al.*, Advanced usage of $Ti_3C_2T_x$ MXenes for photothermal therapy on different 3D breast cancer models, *Biomed. Pharmacother.*, 2022, **153**, 113496.

30 Y. Jiang, J. Li, X. Zhen, C. Xie and K. Pu, Dual–peak absorbing semiconducting copolymer nanoparticles for first and second near–infrared window photothermal therapy: a comparative study, *Adv. Mater.*, 2018, **30**, 1705980.
31 R. Vankayala and K. C. Hwang, Near–infrared–light–activatable nanomaterial–mediated phototheranostic nanomedicines: an emerging paradigm for cancer treatment, *Adv. Mater.*, 2018, **30**, 1706320.
32 P. A. Rasheed, R. P. Pandey, F. Banat and S. W. Hasan, Recent advances in niobium MXenes: Synthesis, properties, and emerging applications, *Matter*, 2022, **5**, 546–572.
33 T. J. Silhavy, D. Kahne and S. Walker, The bacterial cell envelope, *Cold Spring Harbor Perspect. Biol.*, 2010, **2**, a000414.
34 K. Kabashima, T. Honda, F. Ginhoux and G. Egawa, The immunological anatomy of the skin, *Nat. Rev. Immunol.*, 2019, 19–30.
35 A. Baroni, E. Buommino, V. De Gregorio, E. Ruocco, V. Ruocco and R. Wolf, Structure and function of the epidermis related to barrier properties, *Clin. Dermatol.*, 2012, 257–262.
36 Q. M. Hu, W. J. Yi, M. Y. Su, S. Jiang, S. Z. Xu and T. C. Lei, Induction of retinal-dependent calcium influx in human melanocytes by UVA or UVB radiation contributes to the stimulation of melanosome transfer, *Cell Proliferation*, 2017, **50**, e12372.
37 A. Pupovac, B. Senturk, C. Griffoni, K. Maniura-Weber, M. Rottmar and S. L. McArthur, Toward Immunocompetent 3D Skin Models, *Adv. Healthcare Mater.*, 2018, **7**, 1701405.
38 A. Opneja, S. Kapoor and E. X. Stavrou, Contribution of platelets, the coagulation and fibrinolytic systems to cutaneous wound healing, *Thromb. Res.*, 2019, **179**, 56–63.
39 N. N. Mahmoud, K. Hamad, A. Al Shibitini, S. Juma, S. Sharifi, L. Gould, *et al.*, Investigating Inflammatory Markers in Wound Healing: Understanding Implications and Identifying Artifacts, *ACS Pharmacol. Transl. Sci.*, 2024, **7**, 18–27.
40 T. K. Hunt, H. Hopf and Z. Hussain, Physiology of wound healing, *Adv. Skin Wound Care*, 2000, **13**, 6.
41 R. F. Pereira and P. J. Bartolo, Traditional therapies for skin wound healing, *Adv. Wound Care*, 2016, **5**, 208–229.
42 K. E. Johnson and T. A. Wilgus, Vascular endothelial growth factor and angiogenesis in the regulation of cutaneous wound repair, *Adv. Wound Care*, 2014, **3**, 647–661.
43 D. Singh, V. Rai and D. K. Agrawal, Regulation of collagen I and collagen III in tissue injury and regeneration, *Cardiol. Cardiovasc. Med.*, 2023, **7**, 5.
44 S. Kimura and T. Tsuji, Mechanical and immunological regulation in wound healing and skin reconstruction, *Int. J. Mol. Sci.*, 2021, **22**, 5474.
45 M. Kharaziha, A. Baidya and N. Annabi, Rational design of immunomodulatory hydrogels for chronic wound healing, *Adv. Mater.*, 2021, **33**, 2100176.
46 J. Bian, F. Cai, H. Chen, Z. Tang, K. Xi, J. Tang, *et al.*, Modulation of local overactive inflammation via injectable hydrogel microspheres, *Nano Lett.*, 2021, **21**, 2690–2698.
47 B. Yuan, Z. Upton, D. Leavesley, C. Fan and X.-Q. Wang, Vascular and collagen target: a rational approach to hypertrophic scar management, *Adv. Wound Care*, 2023, **12**, 38–55.
48 M. Ahn, W.-W. Cho, W. Park, J.-S. Lee, M.-J. Choi, Q. Gao, G. Gao, D.-W. Cho and B. S. Kim, 3D biofabrication of diseased human skin models in vitro, *Biomater. Res.*, 2023, **27**, 80.
49 S. He, Z. Wang, R. Wang, B. Chi, Y. Wang, L. Bu, *et al.*, Current status and perspectives for 3D biomimetic epidermal tissue: from tissue reconstruction to biomedical application, *J. Drug Delivery Sci. Technol.*, 2024, **97**, 105722.
50 D. S. Masson-Meyers, T. A. M. Andrade, G. F. Caetano, F. R. Guimaraes, M. N. Leite, S. N. Leite, *et al.*, Experimental models and methods for cutaneous wound healing assessment, *Int. J. Exp. Pathol.*, 2020, 21–37.
51 H. Li, M. Mu, B. Chen, L. Zhou, B. Han and G. Guo, MXene-based nanomaterials for antibacterial and wound healing, *Mater. Res. Lett.*, 2024, **12**, 67–87.
52 R. Luo, J. Dai, J. Zhang and Z. Li, Accelerated skin wound healing by electrical stimulation, *Adv. Healthcare Mater.*, 2021, **10**, 2100557.
53 X. Xu, S. Wang, H. Wu, Y. Liu, F. Xu and J. Zhao, A multimodal antimicrobial platform based on MXene for treatment of wound infection, *Colloids Surf., B*, 2021, **207**, 111979.
54 X. Zhu, Y. Zhu, K. Jia, B. S. Abraha, Y. Li, W. Peng, *et al.*, A near-infrared light-mediated antimicrobial based on Ag/Ti 3 C 2 T x for effective synergetic antibacterial applications, *Nanoscale*, 2020, **12**, 19129–19141.
55 H. Park, J.-U. Kim, S. Kim, N. S. Hwang and H. D. Kim, Sprayable Ti_3C_2 MXene hydrogel for wound healing and drug release system, *Mater. Today Bio*, 2023, **23**, 100881.
56 C. Liang, H. Wang, Z. Lin, C. Zhang, G. Liu and Y. Hu, Augmented wound healing potential of photosensitive GelMA hydrogel incorporating antimicrobial peptides and MXene nanoparticles, *Front. Bioeng. Biotechnol.*, 2023, **11**, 1310349.
57 M. Liu, L. Zheng, K. Zha, Y. Yang, Y. Hu, K. Chen, *et al.*, Cu(II)@ MXene based photothermal hydrogel with antioxidative and antibacterial properties for the infected wounds, *Front. Bioeng. Biotechnol.*, 2023, **11**, 1308184.
58 Y. Su, X. Zhang, Y. Wei, Y. Gu, H. Xu, Z. Liao, *et al.*, Nanocatalytic hydrogel with rapid photodisinfection and robust adhesion for fortified cutaneous regeneration, *ACS Appl. Mater. Interfaces*, 2023, **15**, 6354–6370.
59 Y. Yang, X. Zhou, Y. K. Chan, Z. Wang, L. Li, J. Li, *et al.*, Photo–activated nanofibrous membrane with self–rechargeable antibacterial function for stubborn infected cutaneous regeneration, *Small*, 2022, **18**, 2105988.
60 X. Zhou, Z. Wang, Y. K. Chan, Y. Yang, Z. Jiao, L. Li, *et al.*, Infection micromilieu–activated nanocatalytic membrane for orchestrating rapid sterilization and stalled chronic

wound regeneration, *Adv. Funct. Mater.*, 2022, **32**, 2109469.

61 H. Li, J. Dai, X. Yi and F. Cheng, Generation of cost-effective MXene@ polydopamine-decorated chitosan nanofibrous wound dressing for promoting wound healing, *Biomater. Adv.*, 2022, **140**, 213055.

62 K. Kasinathan, Y.-K. Park, B. Ravindran, K. Marimuthu, G. Munuswamy-Ramanujam, S. W. Chang, *et al.*, Synergistically self-assembled 2D nanosheets of MXene@ MOF derived CoW-LDH into 3D frameworks functionalized with chitosan for improved skin wound healing, *Chem. Eng. J.*, 2024, **482**, 149088.

63 X. Kang, Y. Li, Z. Duan, X. Shen, R. Fu and D. Fan, A Mxene@ TA/Fe dual-nanozyme composited antifouling hydrogel for burn wound repair, *Chem. Eng. J.*, 2023, **476**, 146420.

64 Z. Wu, S. Li, X. Qin, L. Zheng, J. Fang, L. Wei, *et al.*, Facile preparation of fatigue-resistant Mxene-reinforced chitosan cryogel for accelerated hemostasis and wound healing, *Carbohydr. Polym.*, 2024, 121934.

65 Y. Huang, X. Wang, B. Luo, P. Jin, Y. Zheng, C. Xu, *et al.*, MXene-NH_2/chitosan hemostatic sponges for rapid wound healing, *Int. J. Biol. Macromol.*, 2024, **260**, 129489.

66 Z. Yang, X. Fu, D. Ma, Y. Wang, L. Peng, J. Shi, *et al.*, Growth Factor–Decorated Ti_3C_2 MXene/MoS_2 2D Bio–Heterojunctions with Quad–Channel Photonic Disinfection for Effective Regeneration of Bacteria–Invaded Cutaneous Tissue, *Small*, 2021, **17**, 2103993.

67 S. Li, B. Gu, X. Li, S. Tang, L. Zheng, E. Ruiz-Hitzky, *et al.*, MXene–Enhanced Chitin Composite Sponges with Antibacterial and Hemostatic Activity for Wound Healing, *Adv. Healthcare Mater.*, 2022, **11**, 2102367.

68 Y. Li, M. Han, Y. Cai, B. Jiang, Y. Zhang, B. Yuan, *et al.*, Muscle-inspired MXene/PVA hydrogel with high toughness and photothermal therapy for promoting bacteria-infected wound healing, *Biomater. Sci.*, 2022, **10**, 1068–1082.

69 S. Liu, D. Li, Y. Wang, G. Zhou, K. Ge, L. Jiang, *et al.*, Flexible, high-strength and multifunctional polyvinyl alcohol/MXene/polyaniline hydrogel enhancing skin wound healing, *Biomater. Sci.*, 2022, **10**, 3585–3596.

70 H. Zhu, W. Dai, L. Wang, C. Yao, C. Wang, B. Gu, *et al.*, Electroactive oxidized alginate/gelatin/MXene ($Ti_3C_2T_x$) composite hydrogel with improved biocompatibility and self-healing property, *Polymers*, 2022, **14**, 3908.

71 L. Mao, S. Hu, Y. Gao, L. Wang, W. Zhao, L. Fu, *et al.*, Biodegradable and electroactive regenerated bacterial cellulose/MXene ($Ti_3C_2T_x$) composite hydrogel as wound dressing for accelerating skin wound healing under electrical stimulation, *Adv. Healthcare Mater.*, 2020, **9**, 2000872.

72 S. Xu, C. Du, M. Zhang, R. Wang, W. Feng, C. Wang, *et al.*, Electroactive and antibacterial wound dressings based on $Ti_3C_2T_x$ MXene/poly (ε-caprolactone)/gelatin coaxial electrospun nanofibrous membranes, *Nano Res.*, 2023, **16**, 9672–9687.

73 N. Zhang, X. Zhang, Y. Zhu, D. Wang, W. Liu, D. Chen, *et al.*, MOF/MXene-loaded PVA/chitosan hydrogel with antimicrobial effect and wound healing promotion under electrical stimulation and improved mechanical properties, *Int. J. Biol. Macromol.*, 2024, **264**, 130625.

74 X. Ju, J. Kong, G. Qi, S. Hou, B. Wang, X. Diao, *et al.*, Photoelectric-driven conductive composite ionogel patch for effective wound healing, *eScience*, 2024, **4**, 100223.

75 Z. Feng, Y. Fu, S. Huang, L. Huang, Y. Zhong, Y. Lai, *et al.*, A MXene ($Ti_3C_2T_x$)-dominated bioelectric responsive and multifunctional Nanoplatform accelerating maxillofacial soft tissue defect repair, *Colloid Interface Sci. Commun.*, 2024, **59**, 100768.

76 L. Sun, L. Fan, F. Bian, G. Chen, Y. Wang and Y. Zhao, MXene-integrated microneedle patches with innate molecule encapsulation for wound healing, *Research*, 2021, **2021**, 9838490.

77 L. Jin, Y. Ma, R. Wang, S. Zhao, Z. Ren, S. Ma, *et al.*, Nanofibers and hydrogel hybrid system with synergistic effect of anti-inflammatory and vascularization for wound healing, *Mater. Today Adv.*, 2022, **14**, 100224.

78 J. Hu, J. Xie, T. Peng, Q. Shi, C. Pan, H. Tan, *et al.*, Fabrication of MXene-Based Shape Memory Hydrogel and Its Application in Skin Wound Repair, *Soft Matter*, 2024, **2021**, 9838490.

79 L. Jin, X. Guo, D. Gao, C. Wu, B. Hu, G. Tan, *et al.*, NIR-responsive MXene nanobelts for wound healing, *NPG Asia Mater.*, 2021, **13**, 24.

80 L. Jin, X. Guo, D. Gao, Y. Liu, J. Ni, Z. Zhang, *et al.*, An NIR photothermal-responsive hybrid hydrogel for enhanced wound healing, *Bioact. Mater.*, 2022, **16**, 162–172.

81 B. Li, W. Yang, R. Shu, H. Yang, F. Yang, W. Dai, *et al.*, Antibacterial and Angiogenic (2A) Bio–Heterojunctions Facilitate Infectious Ischemic Wound Regeneration via an Endogenous–Exogenous Bistimulatory Strategy, *Adv. Mater.*, 2024, **36**, 2307613.

82 X. Wang, Y. Yu, C. Yang, L. Shang, Y. Zhao and X. Shen, Dynamically responsive scaffolds from microfluidic 3D printing for skin flap regeneration, *Adv. Sci.*, 2022, **9**, 2201155.

83 D. Wu, X. Shou, Y. Yu, X. Wang, G. Chen, Y. Zhao, *et al.*, Biologics–loaded photothermally dissolvable hyaluronic acid microneedle patch for psoriasis treatment, *Adv. Funct. Mater.*, 2022, **32**, 2205847.

84 M. Zheng, X. Wang, J. Zhang, O. Yue, J. Zhang, Z. Bai, *et al.*, Nature-skin-derived multi-responsive e-skin as on-demand drug-delivery system facilitated melanoma post-operative therapy, *J. Mater. Sci. Technol.*, 2024, **188**, 155–168.

85 M. Li, Y. Zhang, L. Lian, K. Liu, M. Lu, Y. Chen, *et al.*, Flexible Accelerated–Wound–Healing Antibacterial MXene–Based Epidermic Sensor for Intelligent Wearable Human–Machine Interaction, *Adv. Funct. Mater.*, 2022, **32**, 2208141.

86 X. Yang, C. Zhang, D. Deng, Y. Gu, H. Wang and Q. Zhong, Multiple stimuli–responsive mxene–based hydrogel as intelligent drug delivery carriers for deep chronic wound healing, *Small*, 2022, **18**, 2104368.

87 S. Wang, S. Bi, L. Zhang, R. Liu, H. Wang and J. Gu, Skin-inspired antibacterial conductive hydrogels customized for wireless flexible sensor and collaborative wound healing, *J. Mater. Chem. A*, 2023, **11**, 14096–14107.

88 Y. Zou, X. Jin, X. Zhang, X. Kong, Q. Zhang, X. Xie, *et al.*, A multifunctional biomedical patch based on hyperbranched epoxy polymer and MXene, *Sci. China: Technol. Sci.*, 2021, **64**, 2744–2754.

89 J. Li and S. Zhuang, Antibacterial activity of chitosan and its derivatives and their interaction mechanism with bacteria: Current state and perspectives, *Eur. Polym. J.*, 2020, **138**, 109984.

90 G. Perini, V. Palmieri, A. Papait, A. Augello, D. Fioretti, S. Iurescia, *et al.*, Slow and steady wins the race: Fractionated near-infrared treatment empowered by graphene-enhanced 3D scaffolds for precision oncology, *Mater. Today Bio*, 2024, 100986.

91 S. Wang, Z. Zhang, S. Wei, F. He, Z. Li, H.-H. Wang, *et al.*, Near-infrared light-controllable MXene hydrogel for tunable on-demand release of therapeutic proteins, *Acta Biomater.*, 2021, **130**, 138–148.

92 J. Chen, F. Liu, H. Liu, T. Wang, Y. Hui, H. Chen, *et al.*, Doped-MXene assists in deciphering metabolic signature of psoriasis and unraveling dysregulated leukotriene metabolism, *Arabian J. Chem.*, 2024, **17**, 105774.

93 L. Sun, Z. Wang, H. Kang, P. Luo, J. Su, W. Wei, *et al.*, A flexibility self-powered Band-Aid for diabetes wound healing and skin bioelectronics, *Chem. Eng. J.*, 2024, **481**, 148096.

94 S. Zhang, G. Ge, Y. Qin, W. Li, J. Dong, J. Mei, *et al.*, Recent advances in responsive hydrogels for diabetic wound healing, *Mater. Today Bio*, 2023, **18**, 100508.

95 S. Zhang, G. Ge, Y. Qin, W. Li, J. Dong, J. Mei, *et al.*, Recent advances in responsive hydrogels for diabetic wound healing, *Mater. Today Bio*, 2023, **18**, 100508.

96 J. L. Burgess, W. A. Wyant, B. Abdo Abujamra, R. S. Kirsner and I. Jozic, Diabetic wound-healing science, *Medicina*, 2021, **57**, 1072.

97 L. Zhou, H. Zheng, Z. Liu, S. Wang, Z. Liu, F. Chen, *et al.*, Conductive antibacterial hemostatic multifunctional scaffolds based on Ti_3C_2T x MXene nanosheets for promoting multidrug-resistant bacteria-infected wound healing, *ACS Nano*, 2021, **15**, 2468–2480.

98 Y. Zhong, Y. Lai, Z. Feng, S. Huang, Y. Fu, L. Huang, *et al.*, Multifunctional MXene-doped photothermal microneedles for drug-resistant bacteria-infected wound healing, *Biomater. Sci.*, 2024, **12**, 660–673.

99 Z. Li, W. Wei, M. Zhang, X. Guo, B. Zhang, D. Wang, *et al.*, Cryptotanshinone–Doped Photothermal Synergistic MXene@ PDA Nanosheets with Antibacterial and Anti–Inflammatory Properties for Wound Healing, *Adv. Healthcare Mater.*, 2023, **12**, 2301060.

100 H. Zheng, S. Wang, F. Cheng, X. He, Z. Liu, W. Wang, *et al.*, Bioactive anti-inflammatory, antibacterial, conductive multifunctional scaffold based on MXene@ CeO_2 nanocomposites for infection-impaired skin multimodal therapy, *Chem. Eng. J.*, 2021, **424**, 130148.

101 H. Yuan, X. Hong, H. Ma, C. Fu, Y. Guan, W. Huang, *et al.*, MXene-based dual functional nanocomposite with photothermal nanozyme catalytic activity to fight bacterial infections, *ACS Mater. Lett.*, 2023, **5**, 762–774.

102 Y. Li, R. Fu, Z. Duan, C. Zhu and D. Fan, Artificial nonenzymatic antioxidant MXene nanosheet-anchored injectable hydrogel as a mild photothermal-controlled oxygen release platform for diabetic wound healing, *ACS Nano*, 2022, **16**, 7486–7502.

103 C. Wei, P. Tang, Y. Tang, L. Liu, X. Lu, K. Yang, *et al.*, Sponge–Like Macroporous Hydrogel with Antibacterial and ROS Scavenging Capabilities for Diabetic Wound Regeneration, *Adv. Healthcare Mater.*, 2022, **11**, 2200717.

104 Y. Dong, J. Liu, Y. Chen, T. Zhu, Y. Li, C. Zhang, *et al.*, Photothermal and natural activity-based synergistic antibacterial effects of Ti_3C_2Tx MXene-loaded chitosan hydrogel against methicillin-resistant Staphylococcus aureus, *Int. J. Biol. Macromol.*, 2023, **240**, 124482.

105 X. Wang, L. Luo, C. Yang, Q. Wang, P. Wang, B. Xu, *et al.*, Disulfide bond network crosslinked flexible multifunctional chitosan coating on fabric surface prepared by the chitosan grafted with thioctic acid, *Int. J. Biol. Macromol.*, 2024, 130431.

106 Y. Fu, Y. Cheng, Q. Wei, Y. Zhao, W. Zhang, Y. Yang, *et al.*, Multifunctional biomass composite aerogel co-modified by MXene and Ag nanowires for health monitoring and synergistic antibacterial applications, *Appl. Surf. Sci.*, 2022, **598**, 153783.

107 Y. Dong, S. Li, X. Li and X. Wang, Smart MXene/agarose hydrogel with photothermal property for controlled drug release, *Int. J. Biol. Macromol.*, 2021, **190**, 693–699.

108 Y. Ding, L. Xu, S. Chen, Y. Zhu, Y. Sun, L. Ding, *et al.*, Mxene composite fibers with advanced thermal management for inhibiting tumor recurrence and accelerating wound healing, *Chem. Eng. J.*, 2023, **459**, 141529.

109 X. Ju, J. Kong, G. Qi, S. Hou, X. Diao, S. Dong, *et al.*, A wearable electrostimulation-augmented ionic-gel photothermal patch doped with MXene for skin tumor treatment, *Nat. Commun.*, 2024, **15**, 762.

110 A. Nosrati, J. G. Berliner, S. Goel, J. McGuire, V. Morhenn, J. R. de Souza, *et al.*, Outcomes of melanoma in situ treated with Mohs micrographic surgery compared with wide local excision, *JAMA Dermatol.*, 2017, **153**, 436–441.

111 K. Phan and A. Loya, Mohs micrographic surgery versus wide local excision for melanoma in situ: analysis of a nationwide database, *Int. J. Dermatol.*, 2019, **58**, 697–702.

112 W. Shi, *Radiation therapy for melanoma*, Exon Publications, 2017, pp. 101–120.

113 E. Yosefof, N. Kurman and D. Yaniv, The role of radiation therapy in the treatment of non-melanoma skin cancer, *Cancers*, 2023, **15**, 2408.

114 S. Vaienti, P. Calzari and G. Nazzaro, Topical Treatment of Melanoma In Situ, Lentigo Maligna, and Lentigo Maligna

Melanoma with Imiquimod Cream: A Systematic Review of the Literature, *Dermatol. Ther.*, 2023, 2187–2215.

115 H. Zhang, X. Li, P. You, X. Song, Q. Fan, X. Tao, *et al.*, Highly tumoricidal efficiency of non-oxidized MXene-$Ti_3C_2T_x$ quantum dots on human uveal melanoma, *Front. Bioeng. Biotechnol.*, 2022, **10**, 1028470.

116 B. Li, G. Fu, C. Liu, Y. Lu, Y. Mi, D. Yan, *et al.*, Ti_2C_3 MXene-based nanocomposite as an intelligent nanoplatform for efficient mild hyperthermia treatment, *J. Colloid Interface Sci.*, 2024, **665**, 389–398.

117 X. Ju, J. Kong, G. Qi, S. Hou, X. Diao, S. Dong, *et al.*, A wearable electrostimulation-augmented ionic-gel photothermal patch doped with MXene for skin tumor treatment, *Nat. Commun.*, 2024, **15**, 762.

118 H. Riazi, G. Taghizadeh and M. Soroush, MXene-based nanocomposite sensors, *ACS Omega*, 2021, **6**, 11103–11112.

119 Y. Liu, D. Xu, Y. Ding, X. Lv, T. Huang, B. Yuan, *et al.*, A conductive polyacrylamide hydrogel enabled by dispersion-enhanced MXene@ chitosan assembly for highly stretchable and sensitive wearable skin, *J. Mater. Chem. B*, 2021, **9**, 8862–8870.

120 B. Yan, X. Bao, X. Liao, P. Wang, M. Zhou, Y. Yu, *et al.*, Sensitive micro-breathing sensing and highly-effective photothermal antibacterial cinnamomum camphora bark micro-structural cotton fabric via electrostatic self-assembly of MXene/HACC, *ACS Appl. Mater. Interfaces*, 2021, **14**, 2132–2145.

121 V. S. Sivasankarapillai, T. S. K. Sharma, K.-Y. Hwa, S. M. Wabaidur, S. Angaiah and R. Dhanusuraman, MXene based sensing materials: current status and future perspectives, *ES Energy Environ.*, 2022, **15**, 4–14.

122 Y. Pei, X. Zhang, Z. Hui, J. Zhou, X. Huang, G. Sun, *et al.*, $Ti_3C_2T_x$ MXene for sensing applications: recent progress, design principles, and future perspectives, *ACS Nano*, 2021, **15**, 3996–4017.

123 F. Hao, L. Wang, B. Chen, L. Qiu, J. Nie and G. Ma, Bifunctional smart hydrogel dressing with strain sensitivity and NIR-responsive performance, *ACS Appl. Mater. Interfaces*, 2021, **13**, 46938–46950.

124 X. Zhao, L.-Y. Wang, C.-Y. Tang, X.-J. Zha, Y. Liu, B.-H. Su, *et al.*, Smart $Ti_3C_2T_x$ MXene fabric with fast humidity response and joule heating for healthcare and medical therapy applications, *ACS Nano*, 2020, **14**, 8793–8805.

125 H. Lu, W. Shao, B. Gao, S. Zheng and B. He, Intestine-inspired wrinkled MXene microneedle dressings for smart wound management, *Acta Biomater.*, 2023, **159**, 201–210.

126 Y. Wang, B. Gao and B. He, Toward efficient wound management: bioinspired microfluidic and microneedle patch, *Small*, 2023, **19**, 2206270.

127 M. Guo, Y. Wang, B. Gao and B. He, Shark tooth-inspired microneedle dressing for intelligent wound management, *ACS Nano*, 2021, **15**, 15316–15327.

128 Y. Shao, K. Dong, X. Lu, B. Gao and B. He, Bioinspired 3D-printed MXene and spidroin-based near-infrared light-responsive microneedle scaffolds for efficient wound management, *ACS Appl. Mater. Interfaces*, 2022, **14**, 56525–56534.

129 X. Luo, Y. Liu, R. Qin, F. Ao, X. Wang, H. Zhang, *et al.*, Tissue-nanoengineered hyperbranched polymer based multifunctional hydrogels as flexible "wounped treatment-health monitoring" bioelectronic implant, *Appl. Mater. Today*, 2022, **29**, 101576.

130 M. Mao, J. Kong, X. Ge, Y. Sun, H. Yu, J. Liu, *et al.*, Mxene-based wearable self-powered and photothermal triboelectric nanogenerator patches for wound healing acceleration and tactile sensing, *Chem. Eng. J.*, 2024, **482**, 148949.

131 D. Liu, S. Bi, H. Wang, J. Gu and S. Wang, Polydopamine interface-modulated MXene-based conductive antibacterial hydrogels for on-skin health monitoring and diabetic wound healing, *Composites, Part A*, 2024, 108065.

132 Y. Jing, T. Huang, B. Zhao, L. Zhao, N. Zhang, K. Zhang, *et al.*, A ROS/glucose stimulated-responsive ADSCs-derived exosomes-release hydrogel system for diabetic wound healing, *Chem. Eng. J.*, 2024, **487**, 150561.

133 M. Li, Y. Zhang, L. Lian, K. Liu, M. Lu, Y. Chen, *et al.*, Flexible Accelerated–Wound–Healing Antibacterial MXene–Based Epidermic Sensor for Intelligent Wearable Human–Machine Interaction, *Adv. Funct. Mater.*, 2022, **32**, 2208141.

134 H. Lu, W. Shao, B. Gao, S. Zheng and B. He, Intestine-inspired wrinkled MXene microneedle dressings for smart wound management, *Acta Biomater.*, 2023, **159**, 201–210.

135 P. R. Cohen and R. Kurzrock, Dermatologic Disease-Directed Targeted Therapy (D_3T_2): The Application of Biomarker-Based Precision Medicine for the Personalized Treatment of Skin Conditions—Precision Dermatology, *Dermatol. Ther.*, 2022, **12**, 2249–2271.

136 L. Fusco, A. Gazzi, C. E. Shuck, M. Orecchioni, D. Alberti, S. M. D'Almeida, *et al.*, Immune profiling and multiplexed label–free detection of 2D MXenes by mass cytometry and high–dimensional imaging, *Adv. Mater.*, 2022, **34**, 2205154.

137 A. Gazzi, L. Fusco, M. Orecchioni, S. Keshavan, Y. Shin, J.-C. Grivel, *et al.*, Immune profiling and tracking of two-dimensional transition metal dichalcogenides in cells and tissues, *Nano Today*, 2024, **54**, 102084.

138 L. Fusco, A. Gazzi, C. E. Shuck, M. Orecchioni, E. I. Ahmed, L. Giro, *et al.*, V_4C_3 MXene immune profiling and modulation of T cell–dendritic cell function and interaction, *Small Methods*, 2023, **7**, 2300197.

139 G. Guo, Z. Liu, J. Yu, Y. You, M. Li, B. Wang, *et al.*, Neutrophil Function Conversion Driven by Immune Switchpoint Regulator against Diabetes–Related Biofilm Infections, *Adv. Mater.*, 2024, **36**, 2310320.

140 A. Choromańska and U. Szwedowicz, Electrochemotherapy of melanoma: What we know and what is unexplored?, *Adv. Clin. Exp. Med.*, 2023, 5–8.

141 L. G. Campana, B. Peric, M. Mascherini, R. Spina, C. Kunte, E. Kis, *et al.*, Combination of pembrolizumab with electrochemotherapy in cutaneous metastases from melanoma: A comparative retrospective study from the

inspect and slovenian cancer registry, *Cancers*, 2021, **13**, 4829.

142 S. Milicevic, M. Cemazar, A. K. Ivancic, G. Gasljevic, M. Bosnjak, G. Sersa, *et al.*, Electrochemotherapy of Melanoma Cutaneous Metastases in Organ Transplant Recipients: A Systematic Review of Preclinical and Clinical Studies, *Int. J. Mol. Sci.*, 2023, **151**, 99–101.

143 P. F. Ferrucci, L. Pala, F. Conforti and E. Cocorocchio, Talimogene laherparepvec (T–vec): An intralesional cancer immunotherapy for advanced melanoma, *Cancers*, 2021, 1–14.

144 B. Ramchatesingh, A. Martínez Villarreal, D. Arcuri, F. Lagacé, S. A. Setah, F. Touma, *et al.*, The use of retinoids for the prevention and treatment of skin cancers: an updated review, *Int. J. Mol. Sci.*, 2022, **23**, 12622.

145 S. Yeroushalmi, J. Y. Shirazi and A. Friedman, New developments in bacterial, viral, and fungal cutaneous infections, *Curr. Dermatol. Rep.*, 2020, **9**, 152–165.

146 M. Papi, D. Pozzi, V. Palmieri and G. Caracciolo, Principles for optimization and validation of mRNA lipid nanoparticle vaccines against COVID-19 using 3D bioprinting, *Nano Today*, 2022, 101403.

147 M. Gu, X. Zhou, J. Shen, R. Xie, Y. Su, J. Gao, *et al.*, High-sensitivity, ultrawide linear range, antibacterial textile pressure sensor based on chitosan/MXene hierarchical architecture, *iScience*, 2024, **27**, 109481.

148 S. Kalasin, P. Sangnuang and W. Surareungchai, Intelligent wearable sensors interconnected with advanced wound dressing bandages for contactless chronic skin monitoring: artificial intelligence for predicting tissue regeneration, *Anal. Chem.*, 2022, **94**, 6842–6852.

149 Z. Pazhouhnia, N. Beheshtizadeh, M. S. Namini and N. Lotfibakhshaiesh, Portable hand–held bioprinters promote in situ tissue regeneration, *Bioeng. Transl. Med.*, 2022, **7**, e10307.

150 N. Hakimi, R. Cheng, L. Leng, M. Sotoudehfar, P. Q. Ba, N. Bakhtyar, *et al.*, Handheld skin printer: in situ formation of planar biomaterials and tissues, *Lab Chip*, 2018, **18**, 1440–1451.